Research and Development Technical Report

ECOM-0112-2

MICROWAVE RECIPROCAL LATCHING FERRITE PHASE SHIFTERS

FINAL REPORT
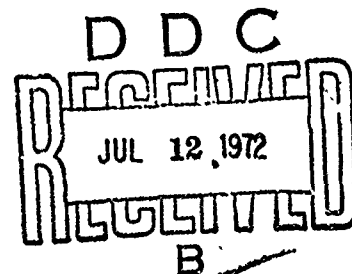
By

R. A. Gaspari   *C. R. Boyd*

June 1972

D D C

JUL 12 1972

B

ECOM

UNITED STATES ARMY ELECTRONICS COMMAND · FORT MONMOUTH, N.J. 07703

CONTRACT DAAB07-71-C-0112

MICROWAVE APPLICATIONS GROUP

Chatsworth, California 91311

NOTICES

Disclaimers

The findings in this report are not to be construed
as an official Department of the Army position, un-
less so designated by other authorized documents.

The citation of trade names and names of manufact-
urers in this report is not to be construed as
official Government endorsement or approval of
commerical products or services referenced herein.

Disposition

Destroy this report when it is no longer needed.
Do not return it to the originator.

DOCUMENT CONTROL DATA - R & D

(Security classification of title, body of abstract and indexing annotation must be entered when the overall report is classified)

1. ORIGINATING ACTIVITY (Corporate author)	2a. REPORT SECURITY CLASSIFICATION
Microwave Applications Group Chatsworth, California 91311	Unclassified
	2b. GROUP

3. REPORT TITLE

Microwave Reciprocal Latching Ferrite Phase Shifters

4. DESCRIPTIVE NOTES (Type of report and inclusive dates)

Final Report   15 September 1971 to 15 June 1972

5. AUTHOR(S) (First name, middle initial, last name)

Russell A. Gaspari and Charles R. Boyd, Jr.

6. REPORT DATE	7a. TOTAL NO. OF PAGES	7b. NO. OF REFS
June 1972	93	7

8a. CONTRACT OR GRANT NO.	9a. ORIGINATOR'S REPORT NUMBER(S)
DAAB07-71-C-0112	ECOM-0112-2
b. PROJECT NO.	
c.	9b. OTHER REPORT NO(S) (Any other numbers that may be assigned this report)
d.	MAG Project J10-010

10. DISTRIBUTION STATEMENT

Approved for public release; Distribution unlimited.

11. SUPPLEMENTARY NOTES	12. SPONSORING MILITARY ACTIVITY
	U.S. Army Electronics Command Fort Monmouth, New Jersey 07703 AMSEL-TL-MM

13. ABSTRACT

In the search for small size, low cost, reciprocal latching microwave phase shifters, two promising designs have been brought to the developmental prototype stage. Each employs a dual mode principle in which contra-rotating senses of circular polarization are subjected to controlled phase delay for opposing directions of propagation. In the first design, the dual mode propagating structure is a ridged waveguide with four equally spaced ridges to maintain double reflection symmetry. In the second design, the dual mode propagating structure is a combination balanced slotline and balanced microstrip both deposited with mutual interaction region within a ferrimagnetic substrate.

The quad ridge waveguide phase shifter had a base insertion loss of 1.5 dB and a latched phase shift of 100° over a range of about 2.9 to 3.3 GHz. The quad ridge geometry proved difficult to match into, and difficult to launch circular polarization into. The length of the rod devoted entirely to phase interaction was 2.3 inches giving a phase efficiency of 43°/inch. Figure of merit at center frequency was 66.7°/dB.

The new and unique slotline/microstrip phase shifter had a base insertion loss of 1.7 dB and a latched phase shift of about 40°. This was achieved with a 5/8 inch long interaction area. Bandwidth extended from 2.5 to 3.0 GHz. This phase shifter design has yet to reach its full potential and is expected to offer very broad bandwidths at very low cost.

Details of illustrations in this document may be better studied on microfiche

Ia

DD FORM 1473 REPLACES DD FORM 1473, 1 JAN 64, WHICH IS OBSOLETE FOR ARMY USE.

14. KEY WORDS	LINK A		LINK B		LINK C	
	ROLE	WT	ROLE	WT	ROLE	WT
Phase Shifter						
Slotline						
Gyromagnetic Coupling						
Coupled Transmission Lines						
Ridged Waveguide						
Ferrite Applications						

$\mathcal{I}h$

MICROWAVE RECIPROCAL LATCHING

FERRITE PHASE SHIFTERS

FINAL REPORT

June 1972

CONTRACT DAAB07-71-C-0112

DISTRIBUTION STATEMENT
Approved for public release
Distribution unlimited

Prepared by

R. A. GASPARI   C. R. BOYD, JR.

MICROWAVE APPLICATIONS GROUP
CHATSWORTH, CALIFORNIA 91311

For

U.S. ARMY ELECTRONICS COMMAND
FORT MONMOUTH, NEW JERSEY 07703

IC

PURPOSE OF CONTRACT

It is the purpose of this contract to research and analyze
approaches suitable for the development of small size, low cost
reciprocal microwave phase shifters, with emphasis on techniques
that may result in significant contributions to the state-of-the-
art in phase shifter design. Additionally, a goal of this contract
is to design, develop, and deliver promising examples of the afore-
mentioned investigation.

ABSTRACT

In the search for small size, low cost, reciprocal latching microwave phase shifters, two promising designs have been brought to the developmental prototype stage. Each employs a dual mode principle in which contra-rotating senses of circular polarization are subjected to controlled phase delay for opposing directions of propagation. In the first design, the dual mode propagating structure is a ridged waveguide with four equally spaced ridges to maintain double reflection symmetry. In the second design, the dual mode propagating structure is a combination balanced slotline and balanced microstrip both deposited with mutual interaction region within a ferrimagnetic substrate.

The quad ridge waveguide phase shifter had a base insertion loss of 1.5 dB and a latched phase shift of 100° over a range of about 2.9 to 3.3 GHz. The quad ridge geometry proved difficult to match into, and difficult to launch circular polarization into. The length of the rod devoted entirely to phase interaction was 2.3 inches giving a phase efficiency of 43°/inch. Figure of merit at center frequency was 66.7°/dB.

The new and unique slotline/microstrip phase shifter had a base insertion loss of 1.7 dB and a latched phase shift of about 40°. This was achieved with a 5/8 inch long interaction area. Bandwidth extended from 2.5 to 3.0 GHz. This phase shifter design has yet to reach its full potential and is expected to offer very broad bandwidths at very low cost.

Preceding page blank

CONTENTS

Preceding page blank

LIST OF ILLUSTRATIONS

Preceding page blank

I
INTRODUCTION

In a continuing effort to produce small size, low cost reciprocal phase shifters for microwave applications, two experimental S-band phase shifter designs have been brought to the development stage. Each is a reciprocal dual mode design. The dual mode transmission line mediums include a unique open sandwich-slotline/balanced-microstrip guiding structure, and a quad ridged waveguide guiding structure. The latter is a refinement of an existing circular waveguide phase shifter design.

Theory behind the dual mode design is fundamental background for each of the two designs. The basis of the theory is use of two non-reciprocal Faraday sections for opposing directions of propagation. In a crude approach this would be achieved using physically distinct phaser sections with circulators at either end, so that by switching the phase shifters in a complementary manner, equal variable insertion phases can be provided for either direction of propagation. In this scheme, illustrated by Figure 1.1, signals passing from left to right are sent through the lower phase shifter, while signals passing from right to left are sent through the upper phase shifter. By switching the phase shifters in a complementary manner, equal variable insertion phases can be provided for either direction of propagation. This approach to achieving reciprocal phase shift with a ferrite component yields the desirable bandwidth, figure of merit, and temperature

1

stability advantages of non-reciprocal phase shifters, except that
it is more complicated and has the additional losses of the input
and output circulators. However, the added complexity can be signif-
icantly reduced by employing a dual-mode transmission system in
which the two non-reciprocal phase shifters operate on two senses
of circular polarization and occupy the same physical space.
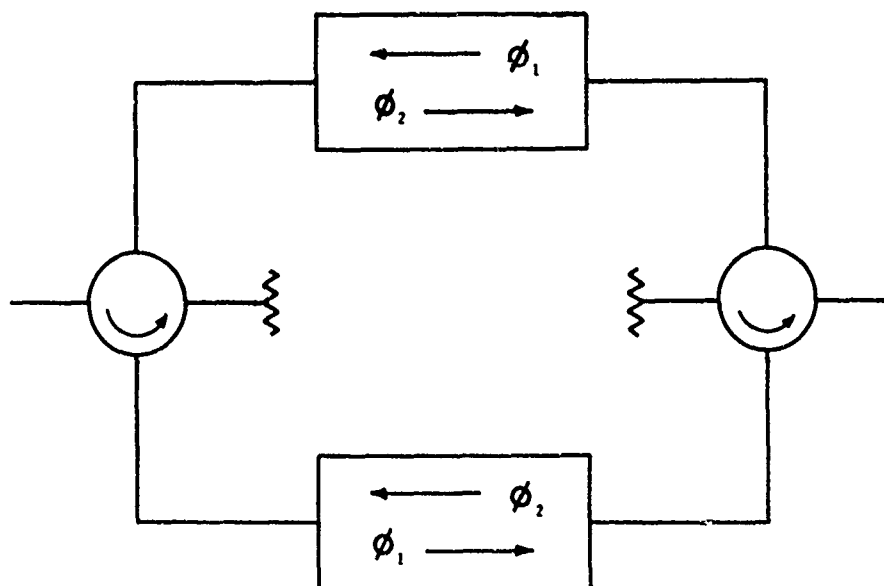
Figure 1.1

Phase shifter block diagram, depicting
the basic concept of the dual channel
phaser.

In order to achieve the desired simplicity, the central phase shift section must have group symmetry properties allowing for the propagation of two degenerate normal modes. In certain propagating media such as free space or square waveguide these properties are easily attained. In a slotline/microstrip composite structure both degeneracy and ellipticity can pose a problem. Analysis of a ferrite loaded multi-mode structure may be achieved in either of two ways, (1) the normal mode approach wherein applied fields are expressed in terms of normal modes of the medium, or (2) the coupled mode approach wherein the propagation effects are expressed in terms of a coupling between modes that has been introduced by the ferrite. In the dual mode Faraday rotation phase shifter design it is helpful to alternate between the two. For example, in the central rotator section with the dual degeneracy of normal modes the normal mode approach is appropriate. In the absence of applied d.c. longitudinal bias field, the degenerate normal modes may be expressed either as a perpendicular linear set (horizontal and vertical)

$$\bar{E}_1 = \bar{u}_x \, f_1(x,y) \qquad \bar{E}_2 = \bar{u}_y \, f_2(x,y)$$

or as a contra-rotating circularly polarized set (right circular polarization or CW·CP and left circular polarization or CCW-CP).

$$\bar{E}_{1,2} = \bar{u}_x \, f_x(x,y) \mp j \, \bar{u}_y \, f_y(x,y)$$

With the application of magnetostatic bias the off diagonal terms of the Polder permeability tensor become non-zero and the proper normal modes become only the circularly polarized set.

3

To utilize this phase shifter design to produce reciprocal phase shift it is necessary to convert incident linear polarized waves into appropriate circular polarized waves. In a waveguide this may be done by providing a physical 45° bend and then inserting a quarter wave plate to delay one component relative to the other. Fur' ,ermore, this transition must be accomplished so that transmit and receive directions are equally delayed by one sense of magnetostatic bias field application. A reproduction of Sakiotis' original sketch (7) is shown in Figure 1.2.

Advantages of this type of iase shifter design are due principally to the efficiency of the basic non-reciprocal component. The advantages of the component is that the bias field operates as a bulk process on all of the transmitted energy which has been totally converted to a circularly polarized normal mode. Of course, the phase drive control of this type of phase shifter design must be of the flux drive type in which selection of a desired phase state is achieved by partial switching of the ferrite from a reference state at either of the extreme remanent flux levels. This partial switching can be accomplished by applying a timed voltage pulse to the switching coil from a low-impedance source.

In the central, variable-field region of this type of phaser design, the ferrite section is long relative to cross section. Thus it is easily magnetized axially and will exhibit remanent magnetization values similar to toroidal shapes if a ferrite yoke is situated external to the interaction region. The circularly polarized wave

4

To antenna

Ferrite 45° rotator

Quarter wave plate

Electronic phase shifter

Quarter wave plate

Ferrite 45° rotator

Generator/receiver

Generated
Signal

Received
Signal
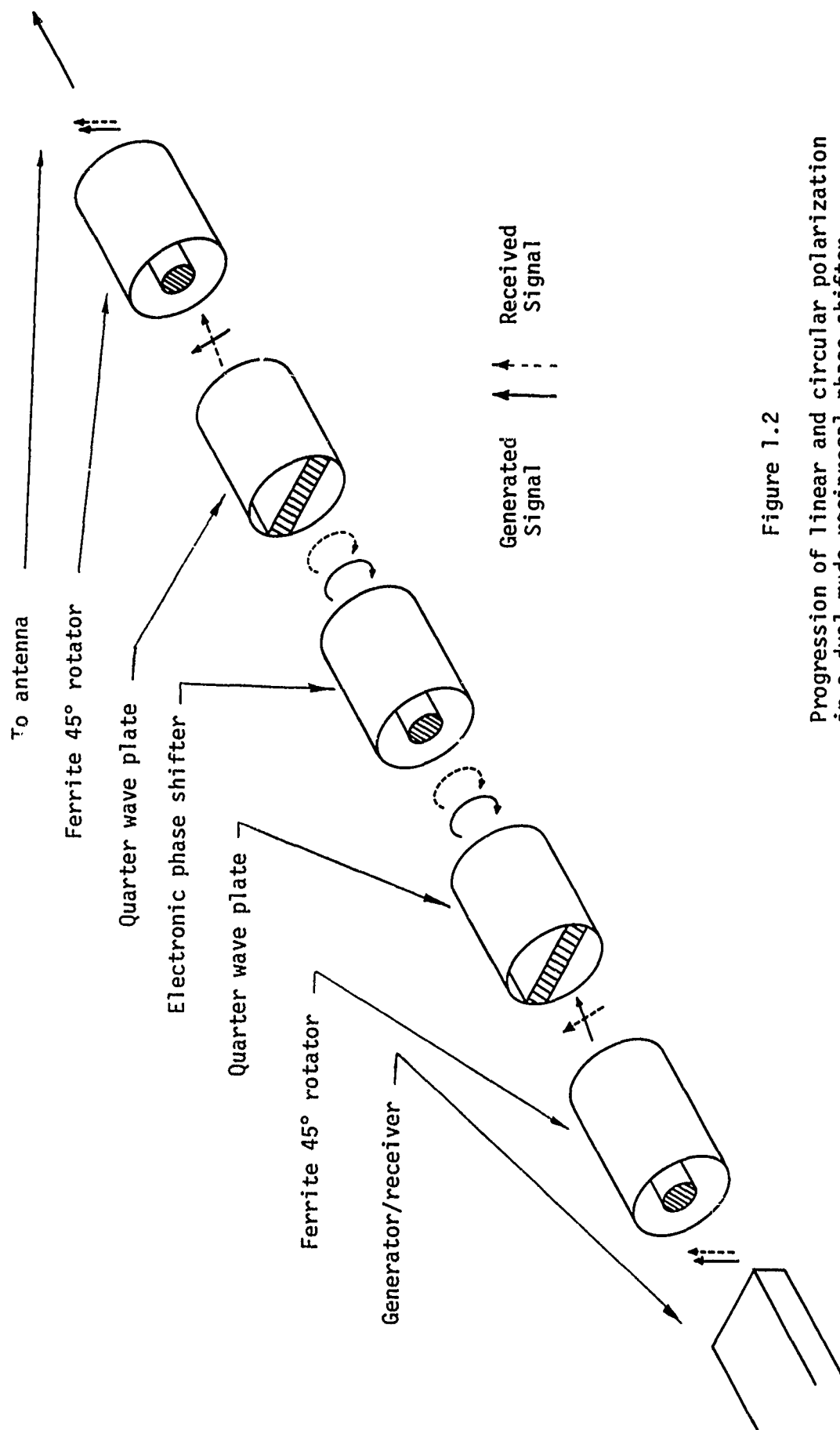
Figure 1.2

Progression of linear and circular polarization
in a dual mode reciprocal phase shifter.
Adapted from Sakiotis (7).

propagating through this section will experience an insertion phase angle that depends upon the saturation moment and the remanent magnetization level of the ferrite. The saturation moment is important because its value relative to the operating frequency affects the magnetic loss and initial permeability of the material. The total available phase shift for the section depends upon the initial permeability and the maximum level of remanent magnetization that can be achieved.

In evaluating the performance of this type of phase shifter it should be noted that the ferrite is never fully magnetized. Because of this the diagonal permeability term μ' will vary with magnetization level and thus affect phase shift. Furthermore, it should be noted that infinite field calculations wherein lossless phase shift ϕ is given by

$$\phi = \gamma\ell = k_0 \sqrt{\mu' \pm \kappa'} \; \ell$$

for circularly polarized waves, will always be greater than for practical waveguide systems because of reduction in the interaction cross section. For symmetric TEM lines

$$\gamma^2 = \omega^2 \mu_0 \varepsilon_0 \left(\mu' \pm \kappa' \frac{\int e \times e'}{\int e \cdot e} \right)$$

where μ' and κ' are real parts of the Polder permeability tensor and e and e' are normalized field amplitudes of the orthogonal modes. Integration over the cross section is assumed. The

6

circular polarizers at either end must then convert an input linear polarization to one sense of circular polarization, while also converting an output opposite sense of circular polarization to normal linear polarization. When the assembled ferrite rod is fitted with a ferrite yoke to permit remanent-magnetization operation, the resulting structure can have size and performance parameters that are well suited to applications in electronic scan array antennas.

In the Semi-Annual Report [1] which documents the first six months efforts on this program, some preliminary investigations were reported which have a bearing on the work reported herein. In that report, three approaches to the miniaturization of phase shifters in the S-band region were investigated. In a ridged waveguide geometry, the cutoff phenomenon was investigated from a transverse resonance viewpoint, and proposed design curves were reported. In a quad balanced line quasi-TEM geometry, rotational properties and theoretical limits were established for potential phaser design. Finally, in a slotline/microstrip geometry, slotline design limits and matching requirements were established, and phase shifter suitability tests were conducted.

In these slotline/microstrip tests, the difference in modal field patterns for the two uncoupled transmission lines induced great care in reducing the elliptical eccentricity as close to unity as possible. Eventually, by optimizing orthogonality and phase velocity, the degree of modal degeneracy was improved to a point wherein 99% of

7

the input excitation mode could be converted to its orthogonal terminated mate.

As a result of these first six months investigations, effort during the most recent six months have concentrated on developing the slotline/microstrip design into a working prototype, with less effort spent on the quad ridged waveguide design. Some rather thorny problems were encountered in each development. In the slotline/ microstrip design, numerous mechanical difficulties were encountered along with the interesting difficulty of obtaining fixed phase shift for the circular polarizers. This fixed phase shift is necessary, as already explained, for the general reciprocal dual mode principle. The fixed phase shift operates on the slotline mode only, and pub- lished literature on slotline theory suggested that this would easily be achieved. This was not found to be the case in practice and a periodic loading technique was eventually employed in the slotline mode to achieve the required polarization. The device length remaining after partitioning to mode division and partial mode delay then led to a limited fixed length available as an interaction area with which to obtain variable phase delay. Because of this, large amounts of phase shift have not yet been obtained in the present design. Unfor- tunately, longer length increases insertion loss which is presently about 1.8 dB for the seven inch effective path length presently in use. Approximately half of this is due to magnetic loss in the garnet since tests with the same geometry deposited on low loss K15 dielectric substrate led to about an 0.9 dB insertion loss.

With the quad ridged waveguide design the principle problem was matching into the ridged waveguide region. An impedance ratio of over 5 to 1 exists between the unloaded waveguide and the fully loaded quad-ridged waveguide. Thus, the impedance translation is critical and must be very carefully designed in order to utilize the bandwidth advantages of a ridged waveguiding structure. Circular polarizers for this type of geometry are more easily constructed than in slotline/microstrip geometry and were achieved by a transversely magnetized quad magnetostatic field.

Each of the two designs has shown considerable promise for application as reciprocal ferrite phase shifters at S-band frequencies. Each, of course, has its limitations. The principle limitation of the slotline/microstrip geometry is high insertion loss due to the unconfined nature of the transmission line propagating structure; and the principle limitation of the quad ridged waveguide design is the slightly added complexity of the manufacturing process.

Contrasting with these limitations, however, each has its advantages. The slotline/microstrip design is low in cost, light in weight, broad in bandwidth, and is easily adaptable to microstrip power distribution schemes. The quad-ridged waveguide design is light in weight and relatively broad in bandwidth.

The two structures developed and described herein were selected as the most promising of the three new approaches first reported in

9

the Semi-Annual Report (1). Of those three techniques for miniaturization of phase shifters in the S-band region, the one discarded was a quadrantally symmetric balanced line. In this approach, gyromagnetic coupling between orthogonal quasi-TEM lines was achieved by utilization of four separate deposited strips of conductors on a quarter-inch square cross section of garnet. It was concluded that the launching of energy into the two orthogonal balanced transmission line systems would introduce prohibitive manufacturing complexity, especially when compared to the slotline/microstrip phaser design. Because of this comparative disadvantage, and because of progressive successes in implementing the slotline/microstrip geometry, the quasi-TEM balanced line phaser does not appear in this report.

II

QUAD RIDGED DUAL MODE PHASE SHIFTER

In a waveguide dual-mode phase shifter, input linearly polarized energy is converted to CP and selectively phase delayed by an externally applied magnetostatic field. A detailed description of the mechanisms of this dual-mode reciprocal design formed the major portion of this paper's Introduction. This design has been implemented in a full height circular waveguide and is commercially available. If the central circular waveguide region is converted to a ridged waveguide then it is possible to lower f_c, the cutoff frequency of the guide, for given transverse size dimensions. Correspondingly, the addition of ridges could lower the transverse dimensions for a given f_c. Because of the nature of the design, it is necessary to maintain point symmetry to insure mode degeneracy and thus the proposed ridges become quad ridges equally spaced around the circumference. A sketch of the design is shown in Figure 2.1. Potential advantages of the new design include lighter weight due to the reduction in size, and broader bandwidth because of the mode separation of ridged guide.

In the semi-annual report a study of the cutoff characteristics of quad-ridged waveguide was presented. The theoretical results of this investigation are re-created in Figure 2.2. In the semi-annual report it was noted that the ridges would substantially reduce the available power handling because of the concentration of field amplitudes in the central axis area between the ridges. Furthermore,

11
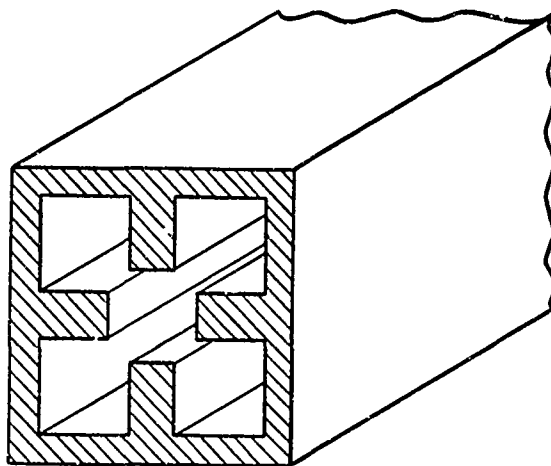
Figure 2.1

Sketch of the Quad-Ridged waveguide in a square geometry.
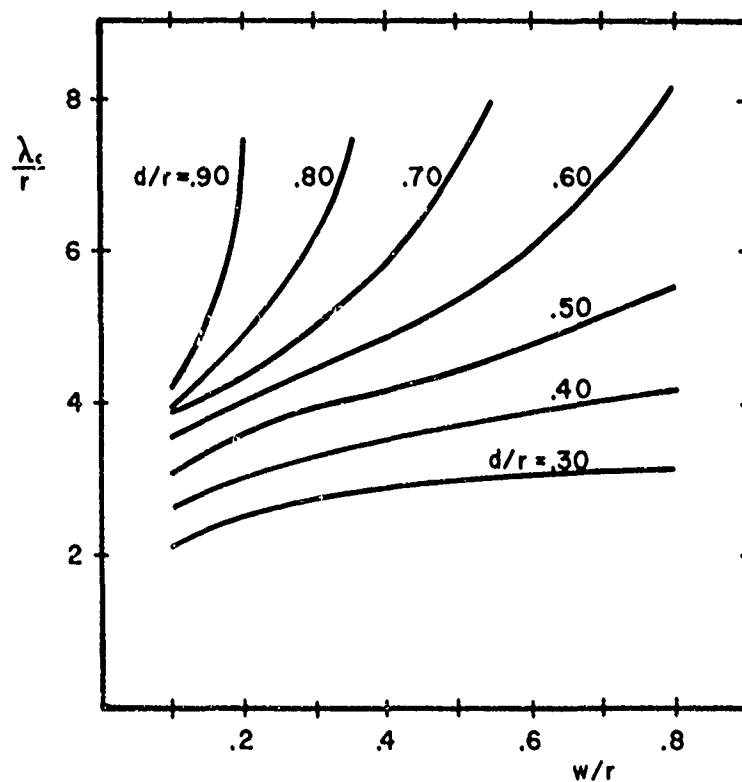
Figure 2.2

Cutoff wavelength ratio of the quadruply ridged circular waveguide as a function of ridge width ratio w/r and ridge depth ratio d/r.

the most significant reduction in waveguide diameter occurs for deep

narrow ridges, and it seems intuitive that the maximum field con-

centration density will increase more rapidly than ridge depth increase.

Thus, in order to have quantitative data on the power effects of the

waveguide ridges, this analytical investigation was inaugurated. The

analysis began by considering a circular geometry into which the

ridges would protrude (reference Figure 2.3). Much later in the

program the difficulty of accurately locating the ridges on a curved

surface led to the square design of Figure 2.1. The four corner

regions of the square ridged geometry were assumed to have minimal

impact on the guide cutoff properties and the "radius" determined by

theory was converted to half width of the square for design purposes.
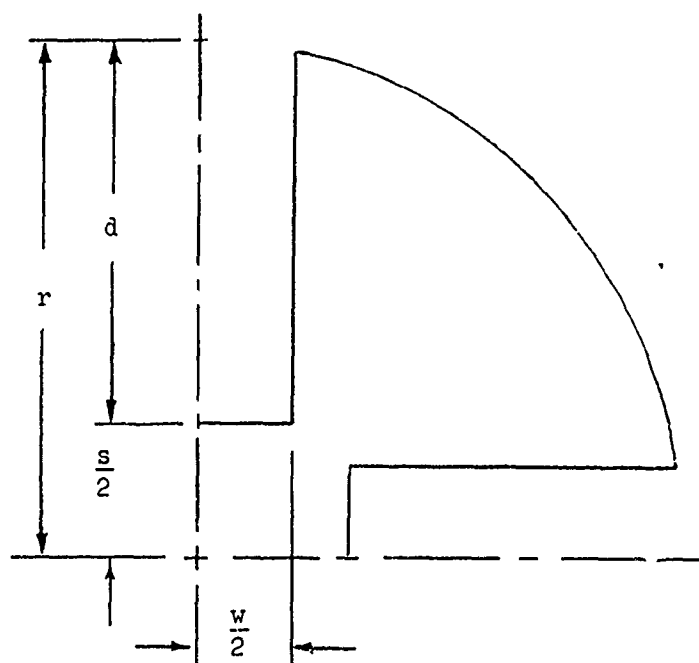
Figure 2.3

Sketch of a portion of the quad ridge waveguide
in a circular geometry showing definitions of
the variables used in the analysis.

13

It will be shown that a power/size trade-off is required for each design. The greater the size reduction, the less the power that the structure can handle. A compromise can be attained at power reduction of 33%. That is, if the full height unridged guide has a power handling capability of P_i then the pow · handling capability of the ridged guide P' will be $P' = 0.33 P_i$.

The power handling capability of the quadrantally ridged waveguide phase shifter is lowered with the addition of the ridges. Two effects are involved, these are the reduction in breakdown potential of the guide itself, and the increase in field concentration to the nonlinearity region of the ferromagnetic material. The power limitation imposed by the latter is over one order of magnitude greater than that of the former at S-band, and is therefore the principle effect of interest.

For a non-ridged, ordinary circular guide, the field distributions for the TE_{mm} modes are

$$H_z = C_0 \, J_n(k_c r) \cos n\phi$$

$$E_r = C_0 \frac{jn\mu f}{k_c r f_c} \, J_n(k_c r) \sin n\phi$$

$$E_\phi = C_0 \frac{jnf}{f_c} \, J'n(k_c r) \cos n\phi$$

$$H_\phi = E_r \frac{1}{n} \left[1 - f_c/f)^2 \right]^{+1/2}$$

$$H_r = -E_\phi \frac{1}{n} \left[1 - (f_c/f)^2 \right]^{+1/2}$$

where C_0 is a constant determined by the magnitude of the field excitation, and the ϕ reference axis is perpendicular to the electric field

maximum of the TE_{11} mode. Subscript n of the TE mode determines angular variations while subscript m determines radial variations and is determined by the root of the derivative of the nth Bessel function.

$$(k_c)_m = \frac{(p'n)_m}{a}$$

A study of the variation of these field magnitudes shows that the maximum magnetic field can occur in either of two critical points. For small f/f_c ratios the magnetic field maximum occurs on the $\phi = 0°$ line as $r \to a$ where a = radius of the circular waveguide. Furthermore, the contribution to this maximum is due solely to the longitudinal component of the magnetic field, H_z, with the other components zero. At large f/f_c ratios the magnetic field maximum occurs on the $\phi = 90°$ line as $r \to 0$. Furthermore, the contribution to this maximum is due solely to H_ϕ since the other components approach zero at this point.

For the TE_{11} mode, these components of interest are

$$H_z = C_0 \, J_1(k_c r) \cos \phi$$

$$H_\phi = C_0 \, [\,'f/f_c)^2 - 1]^{1/2} \, j \, \frac{J_1(k_c r')}{k_c r} \, \sin \phi$$

and the maximum field intensity is the Max between H_z at r=a, $\phi=0°$ and H_ϕ at $r=0^-$, $\phi=90°$. Since

$$v \equiv \lim_{r \to 0} \frac{J_1(k_c r)}{k_c r} = \lim_{r \to 0} \frac{J_r(k_c r) - \frac{1}{k_c r} J_1(k_c r)}{1} = 1 - \lim_{r \to 0} \frac{J_1(k_c r)}{k_c r}$$

then by implication $v = 1/2$ and

$$H_{MAX} \propto \text{Max} \{1/2 \, [f/f_c]^2 - 1]^{1/2}; \, J_1(2\pi a/\lambda_c)\}$$

These two are equal at the crossover point

$$\frac{f}{f_c} = 1.534$$

It is interesting to note that the ratio of the cutoff frequencies of the next two higher order modes compared to the cutoff frequency of the TE_{11} mode are

$$\frac{f_c \, (TM_{01})}{f_c \, (TE_{11})} = 1.306$$

and

$$\frac{f_c \, (TE_{21})}{f_c \, (TE_{11})} = 1.659$$

Although the modal patterns of the magnetized ferrite loaded waveguide will not be identical to those of its non-magnetized counterpart, certain conclusions can be drawn regarding power handling capability. First, the maximum magnetic field amplitude will be a constant function of waveguide radius up the crossover frequency determined by $f/f_c = 1.534$ after which it will increase with frequency. Second, operating at a frequency such that $f/f_c = 1.534$ would allow the second higher order TM_{01} mode to propagate but not the third higher order TE_{21} mode.

16

Above cutoff, the power handling capability of the closed conductor structure can be calculated in terms of the field components by integrating the axial component of the Poynting vector over the cross-sectional area.

$$P = \int_S \bar{E} \times \bar{H} \cdot \overline{ds}$$

and the time average real power is

$$p = \int_S \frac{1}{2} \, \text{Re} \, \{\bar{E} \times \bar{H}^*\}_z \, ds$$

$$= \int_0^{2\pi} \int_0^a \frac{1}{2} \, \text{Re} \, \{E_r H_\phi^* - E_\phi H_r^*\} \, r \, dr \, d\phi$$

thus this may be reduced to

$$p = \int\int \frac{1}{2} \frac{1}{Z_{TE}} |E_t|^2 \, ds$$

then, since all transverse components of a TE wave can be written in terms of H_z, it is possible to write this as

$$p = \int \frac{1}{2Z_{TE}} \frac{\gamma^2}{k_c^2} |\nabla_t H_z|^2 \, ds$$

which can be reduced further by use of the two-dimensional divergence theorem

$$\int \nabla \cdot \bar{A} \, ds = \int \bar{A} \cdot n \, dl$$

with $A = H_z \nabla_t H_z$, and S defined to be the surface of the cylindrical waveguide wall. Then

$$\int (\nabla_t H_z)^2 \, ds = k_c^2 \int H_z^2 \, ds$$

and the power expression becomes

$$p = \frac{n^2(f/f_c)^2}{2Z_{TE}} \int H^2_z \, ds$$

$$p = \frac{n}{2} \left(\frac{f}{f_c}\right)^2 \sqrt{1 - (f_c/f)^2} \int_o^{2\pi} \int_o^a [J_n(k_c r) \cos n\phi]^2 \, r \, dr \, d\phi$$

$$p = \frac{n}{2} \left(\frac{f}{f_c}\right)^2 \sqrt{1 - (f_c/f)^2} \, \pi \left\{ \frac{a^2}{2} \left[J_n'^2(k_c a) + \left(1 + \frac{n^2}{k_c^2 a^2}\right) J_n^2(k_c a) \right] \right\}$$

since the normal derivative of H_z must be zero at the waveguide
boundary, $J_n'(k_c a) = 0$ and this reduces to

$$p = \frac{1}{4} n \frac{f}{f_c} \sqrt{\left(\frac{f}{f_c}\right)^2 - 1} \, \pi a^2 \left(1 + \frac{n^2}{k_c^2 a^2} J_n^2(k_c a)\right)$$

The implication here is that higher ratios of f/f_c correspond to higher
net average power flow for a given mode in a fixed radius waveguide.

As the circularly symmetric waveguide is perturbed by the addition
of ridges, the power handling capacity decreases because the field
amplitudes become more concentrated. If the material remains the
same, then the instability threshhold for a sample magnetized to
saturation is

$$h_{crit} = C \, \frac{\omega}{\omega_M} \, \Delta H_k$$

where ΔH_k is the spin wave linewidth and C is a function of geometry
and internal magnetic field. Since $C \approx 1$, and ΔH_k varies but slightly
with frequency or magnetization, the principle variable is frequency.

18

The ridges will cause an increase in radial electric field component E_r at $\phi = 90°$ varying approximately as $1/s$ where s is the separation between top and bottom ridges. H_ϕ will thus vary accordingly while H_z will largely be unaffected. The maximum magnetic field intensity available to exceed the instability threshhold h_{crit} is then given by

$$H_{MAX} = C_0 MAX \left\{ \frac{a}{s} \left[(f/f_c)^2 - 1 \right]^{1/2} ; J_1 (2\pi a/\lambda_c) \right\}$$

where a is the waveguide radius and d is the ridge depth related to the ridge separation by $d = r - s/2$ (cf. Figure 2.3). A plot of H_{MAX}/C_0 is shown in Figure 2.4.

By studying separately the power limit curve (H_{MAX}/C_0) and the cutoff wavelength curve (λ_c/r) the nature of the power/size tradeoff can be demonstrated.

From the maximum field magnitude curves, one would expect that the ridge separation should not be allowed to decrease to 0.8. A good design goal appears to be $s/r = 1.2$ which produces lowest maxima for $f/f_c < 1.2$ and has a reasonable H_{MAX} maximum for f/f_c as high as 1.5. Unfortunately, no significant decrease in λ_c/r is predicted for these ridge dimensions.

On the other hand, from the cutoff wavelength curves, a 30% reduction in waveguide radius would correspond to

$$\frac{\lambda_c}{r'} = \frac{\lambda_c}{.7 \, r_0} = \frac{3.41}{.7} = 4.9$$
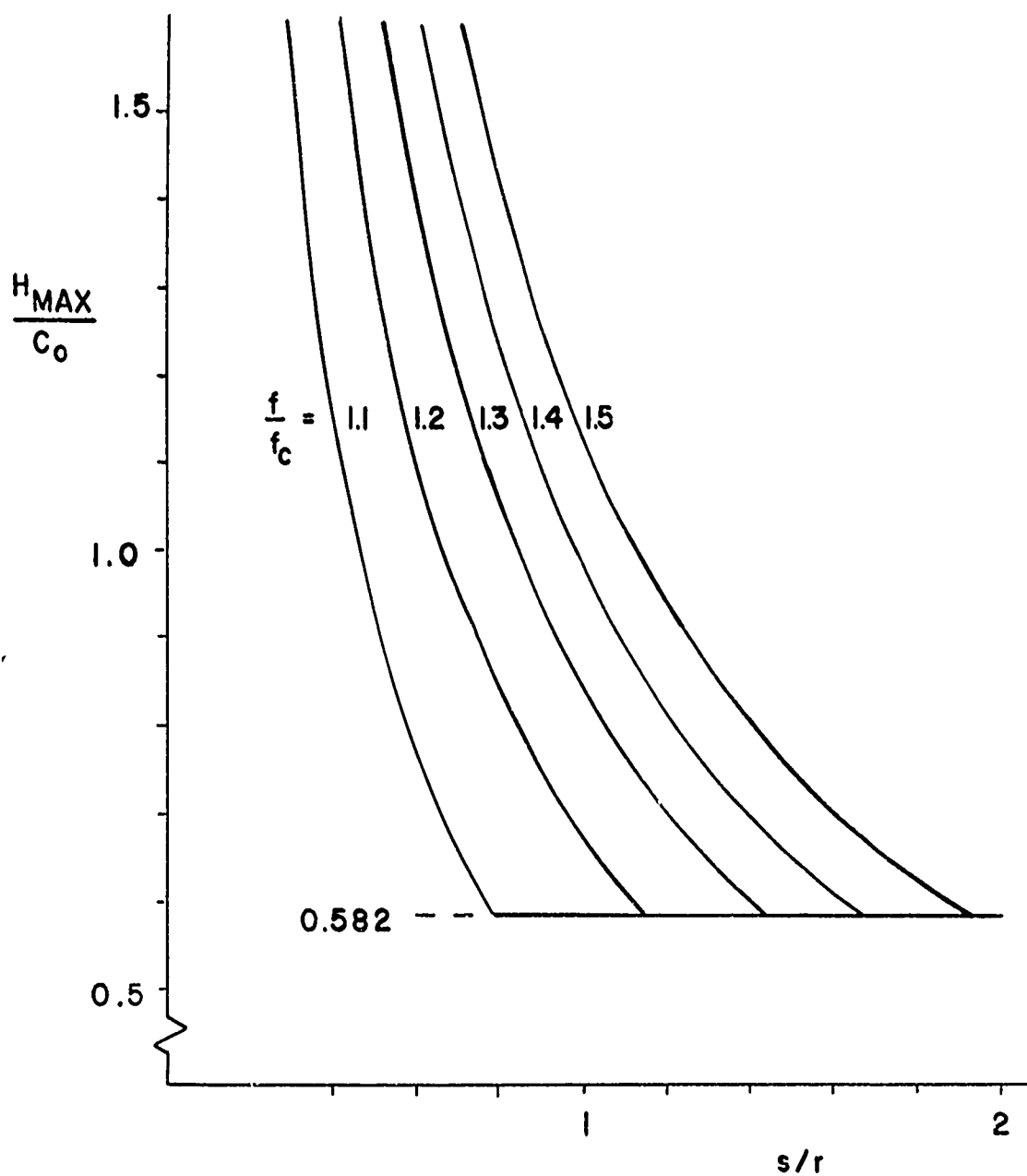
19

Figure 2.4

Normalized maximum magnetic field intensity
of the quadruply ridged circular waveguide
as a function of ridge separation ratio s/r
for various values of frequency. This data
may be used to determine the maximum theor-
etical power handling capability of a specific
quad ridge design.

which could be achieved by ridges of dimensions $w/r = 0.3$ and $d/r = 0.7$. However a depth of 0.7 corresponds to a ridge separation of

$$\frac{s}{r} = 2 \left(1 - \frac{d}{r}\right)$$

or $s/r = 0.6$, which according to the power limit curves could produce very high field amplitudes. A trade-off is obviously necessary.

To assist in these trade-off procedures a standard design technique can be devised. If a percentage limit α is placed on the power handling capability of the ridged guide compared to its unridged counterpart, and if the operating frequency ratio f/f_c does not exceed 1.5, then the allowable ridge separation s/r can be calculated from the H_{MAX} limit.

The time average power flow within the waveguide is proportional to C^2_0 which is the postulated field excitation amplitude. If h_{crit} denotes the instability threshhold then the magnetic field will reach this critical point when

$$C_0 \text{ Max } \left\{ \frac{a}{d} \sqrt{(f/f_c)^2 - 1} \ ; \ J_1 (2\pi a/\lambda_c) \right. = h_{crit}$$

then

$$C_0 = \frac{h_{crit}}{\text{Max } \left\{ \frac{a}{d} \sqrt{(f/f_c)^2 - 1} \ ; \ J_1(2\pi a/\lambda_c) \right\}}$$

so the average power capability is directly proportional to h^2_{crit} and inversely proportional to H^2_{MAX}. So now, if the new requirement P' is α times the unridged guide power P, while the frequency and h_{crit} remain the same, then

$$\frac{H_{MAX}}{H'_{MAX}} = \sqrt{\alpha}$$

and s/r can be determined accordingly. Lastly the ridge width can be determined to achieve a desired reduction in overall guide diameter.

Armed with this design approach, two quad ridge waveguide geometries were designed. In the first design the power ratio α was arbitrarily set at 0.33 while the size reduction was set at 68%. For the un-ridged guide, assuming $f/f_c < 1.534$, the maximum field would be $H_{MAX}/C_0 = 0.582$. To maintain a power ratio of 0.33, the new maximum field in the quadruply ridge region will be

$$\frac{H'_{MAX}}{C_0} = \frac{1}{\sqrt{\alpha}} \quad \frac{H_{MAX}}{C_0} = \frac{1}{\sqrt{1/3}} \ 0.582 = 1.010$$

From the magnetic field curves (Figure 2.4), if f/f_c is held to less than 1.3 then it is possible to achieve this power requirement with an s/r ratio of 0.9. Then

$$\frac{d}{r} = 1 - \frac{1}{2}\frac{s}{r} = 0.55$$

Using next the cutoff wavelength curves (Figure 2.2) an appreciable size reduction of $\lambda_c/r = 5.0$ can be achieved if $w/r = 0.53$, at of course $d/r = 0.55$. Since $\lambda_c/r = 3.41$ for unloaded circular waveguide prop-agating the TE_{11} mode this would correspond to a size reduction of about 68% for equivalent λ_c. At S-band center using 800 Gauss garnet the resultant ridge dimensions are a width of 0.172 inch and a depth of 0.178 inch. The exterior was subsequently converted to square

cross section one side of which was fixed at the previously calculated diameter of 0.65 inch.
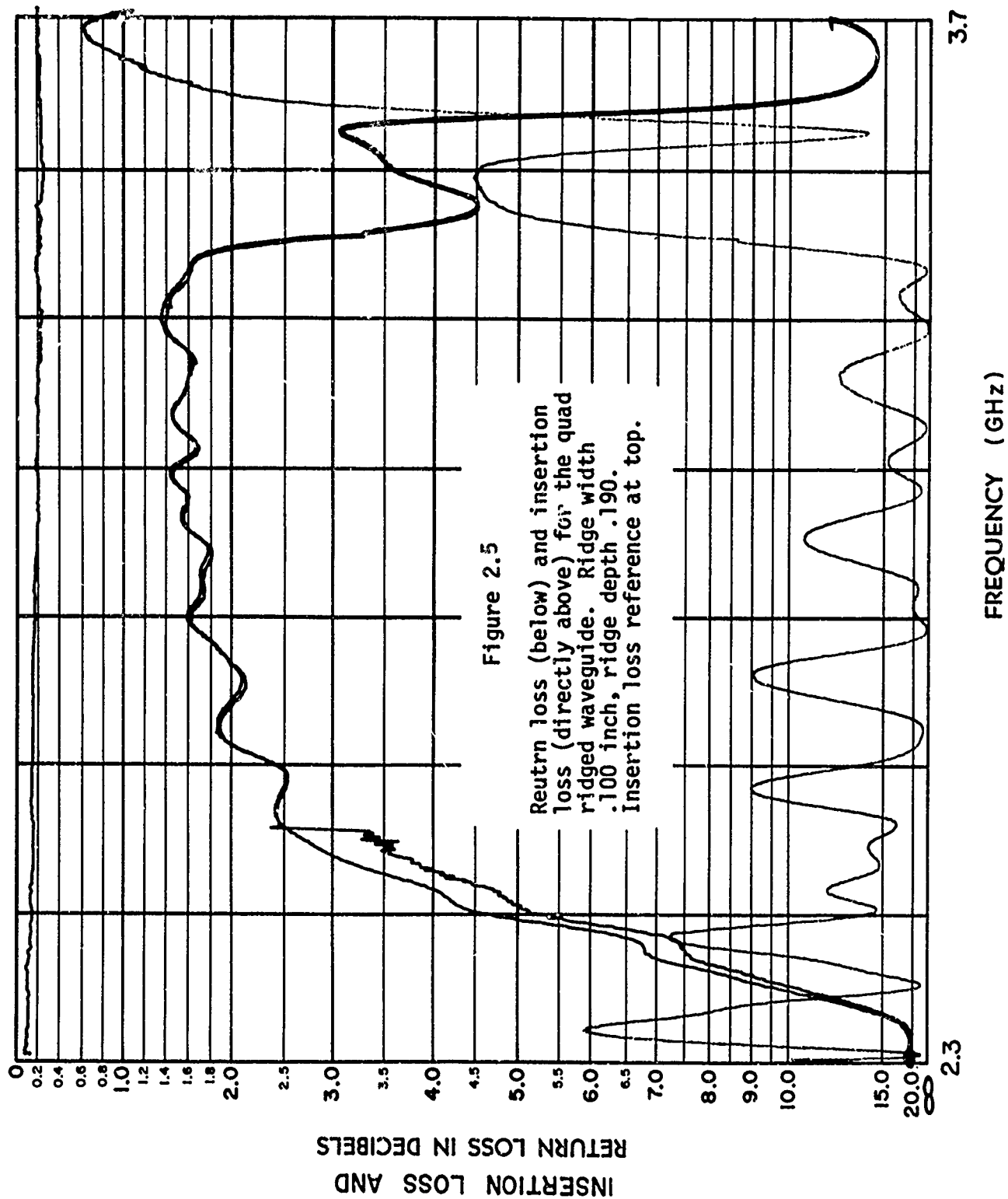
Later, the power requirement was relaxed so that deeper and hence thinner ridges could be employed. With f_c fixed at 2.2 GHz and guide width fixed at 0.65, then λ_c/r = 4.83. A convenient width of .100 inch then led to ratios w/r = .307 and s/r = .82. With ridge separation s/r = .82 then ridge depth is d = .192 inch.

Eventually each of these structures, i.e. ridge width .172 and ridge width .100, was matched as exemplified by Figure 2.5. The minimum insertion loss of each structure was markedly differently, however, being 6 dB for the former (.172 x .178 ridge) and only 1.2 dB for the latter (.100 x .190 ridge). Matching was achieved by a four section transformer, three sections of which consisted of dielectric plug loaded waveguide (see Appendix A) and one section consisted of a quad ridged region of dielectric specifically selected to have a dielectric constant of 11.6. The insertion loss which is clearly depicted in Figure 2.5 is a linear unmagnetized measurement taken before the application of polarizing or phase control fields. The polarizing technique involves the utilization of a quadrupole transverse field which raises the resonance loss frequency of the ferrimagnetic material. An example of the effect of increasing transverse magnetization is shown in Figure 2.6. The bandwidth is limited at the upper end by TE_{21} mode cutoff and limited at the lower end by domain rotation resonance or low field loss. Then increasing the

transverse magnetization begins to creep the resonance loss higher in frequency until the effective bandwidth becomes considerably narrowed. With the 800 Gauss material in use, the insertion loss increases to 8 dB when sufficient transverse magnetization is applied to achieve proper polarization.

However, in spite of the high loss the unit continues to function as a latching reciprocal phase shifter, and a sample hysteresis curve is shown in Figure 2.10. The unit shows 100° of latching phase shift. The interaction coil length to achieve this is 1.9 inches long. To evaluate the available latching phase over an operable frequency band, the swept frequency trace of Figure 2.7 was taken. The available latching phase for any frequency is the difference between the two lines. To verify the reciprocity, Figures 2.8 and 2.9 were recorded. Figure 2.8 shows the frequency variation of the long or RESET state as can be seen by comparison to the lower of the two traces in Figure 2.7. The similar trace superimposed on it demonstrates the same latch state frequency variation for the inverted sense of propagation. Figure 2.9 demonstrates similar uniformity for the short or SET state.

Because of the high insertion loss of the completed unit, a new phase shifter was assembled using identical cross section geometry but using 600 Gauss garnet material (Xtalonix X606). The increase in insertion loss with the application of transverse field (cf. Figure 2.6) is due solely to absorption effects or magnetic loss. The possibility

Figure 2.5

Reutrn loss (below) and insertion loss (directly above) for the quad ridged waveguide. Ridge width .100 inch, ridge depth .190. Insertion loss reference at top.

FREQUENCY (GHz)

INSERTION LOSS AND RETURN LOSS IN DECIBELS

Figure 2.6

Insertion loss of the quad ridged waveguide for various levels of transverse magnetization. By raising the resonance loss frequency in this way the effective bandwidth can be lowered or even eliminated.

FREQUENCY (GHz)

INSERTION LOSS (DB)

26

INSERTION PHASE INCREASE IN DEGREES (50° per inch)

FREQUENCY

3.2

3.8

Figure 2.7

Latched phase state variation with frequency. This trace requires driving the phaser to the saturation extremes of the hysteresis loop and then relaxing back to zero excitation.
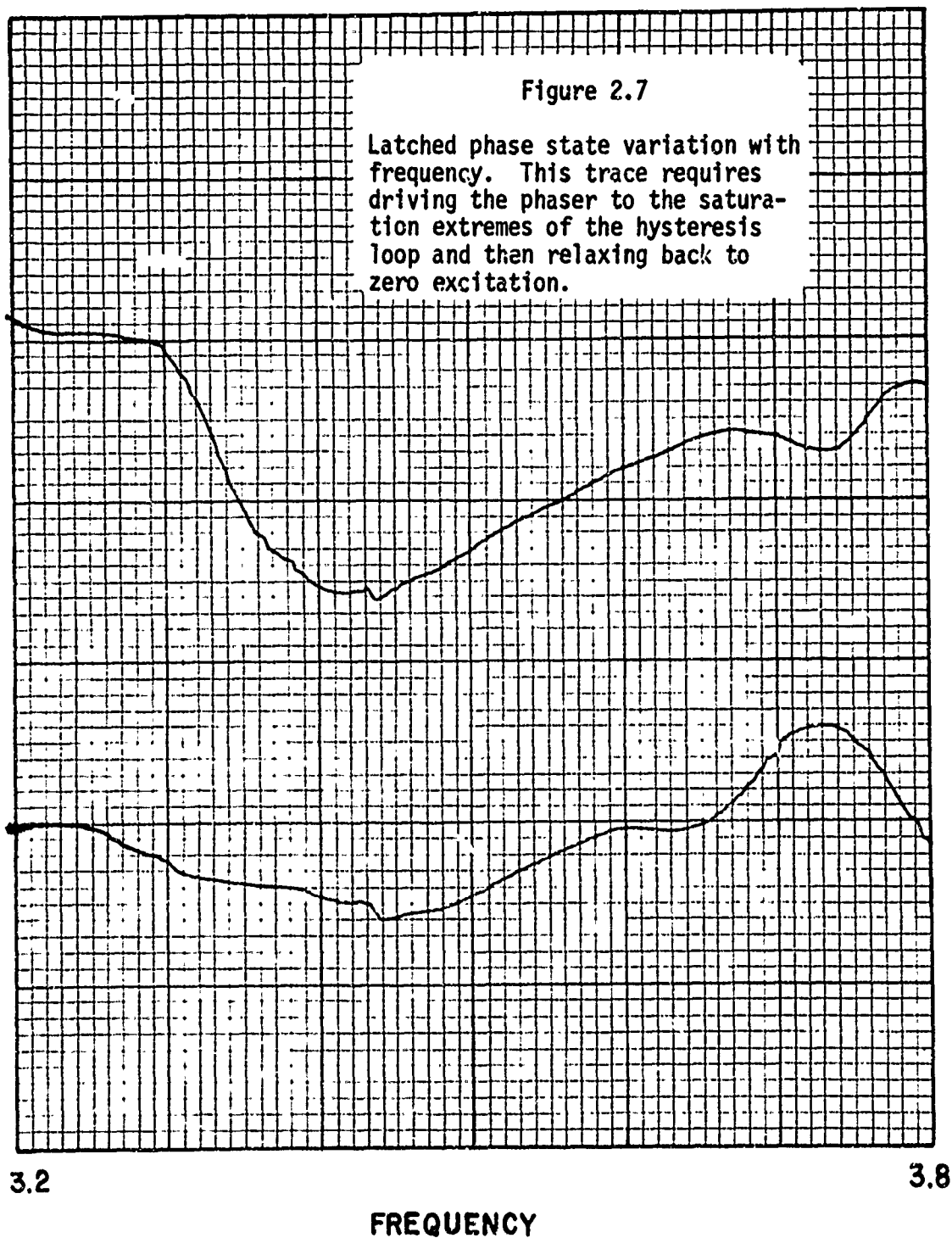
27

INSERTION PHASE INCREASE IN DEGREES (50° per inch)

Figure 2.8

Reciprocity of the "long" latched phase state. The two traces represent frequency variation of the latched phase state for opposing senses of propagation

3.2   3.8

FREQUENCY

28

INSERTION PHASE INCREASE IN DEGREES (50° per inch)

FREQUENCY

3.2   3.8

Figure 2.9

Reciprocity of the "short" latched phase state as a function of frequency.
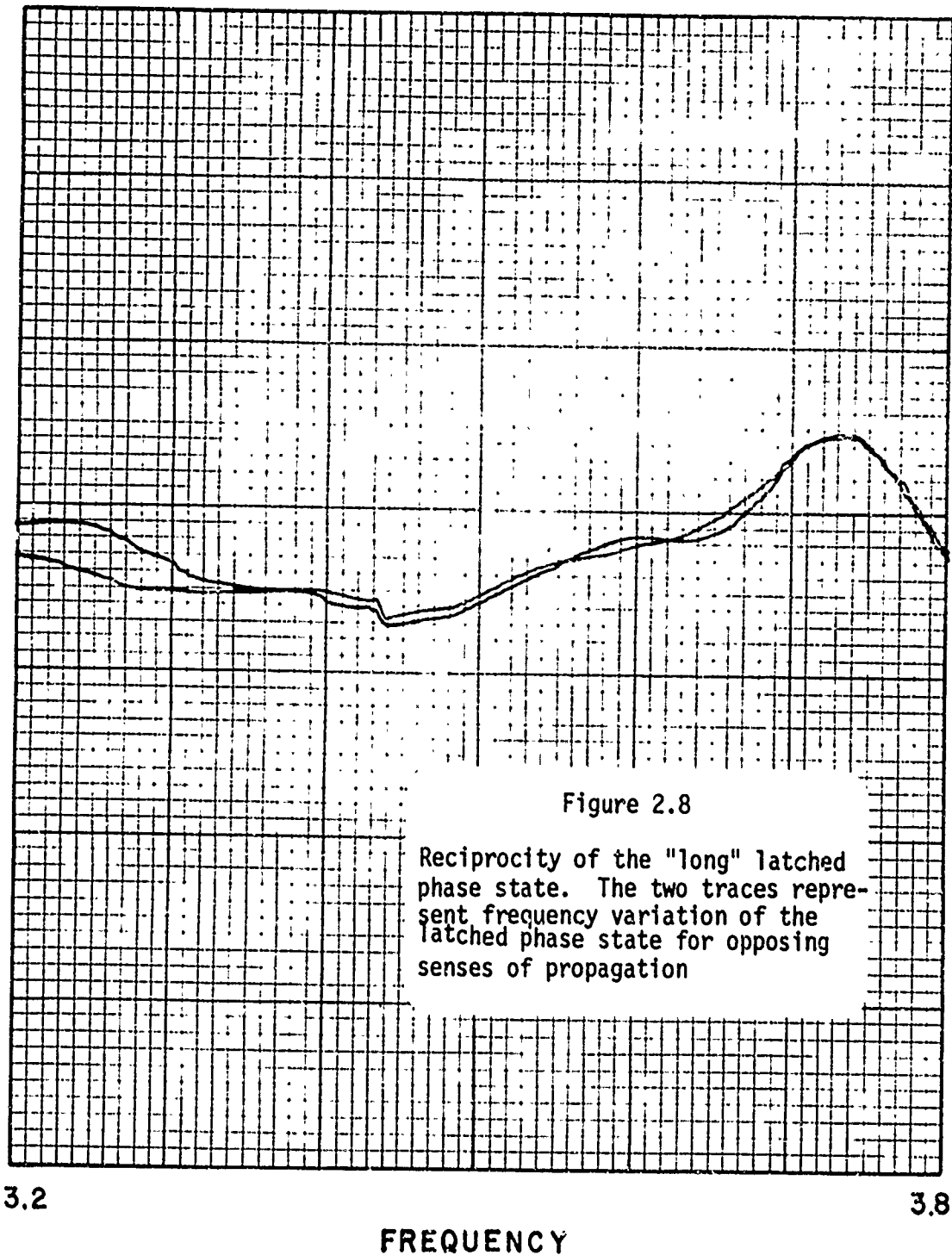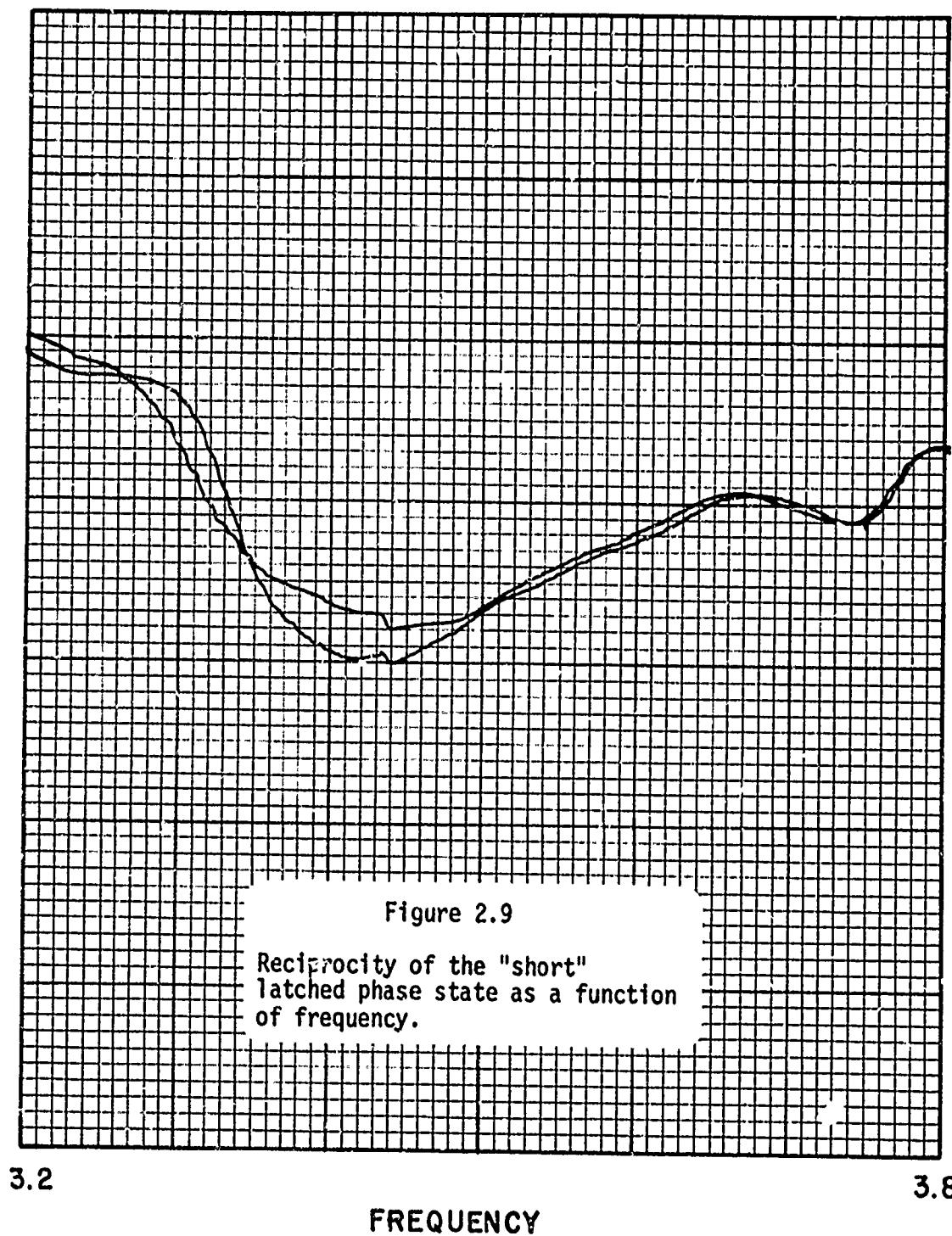
INSERTION PHASE INCREASE IN DEGREES (100° per inch)

Figure 2.10

Hysteresis curve of the completely assembled quad ridge phase shifter measured at 3.5 GHz.

-1A   0   +1A

DRIVE CURRENT

30
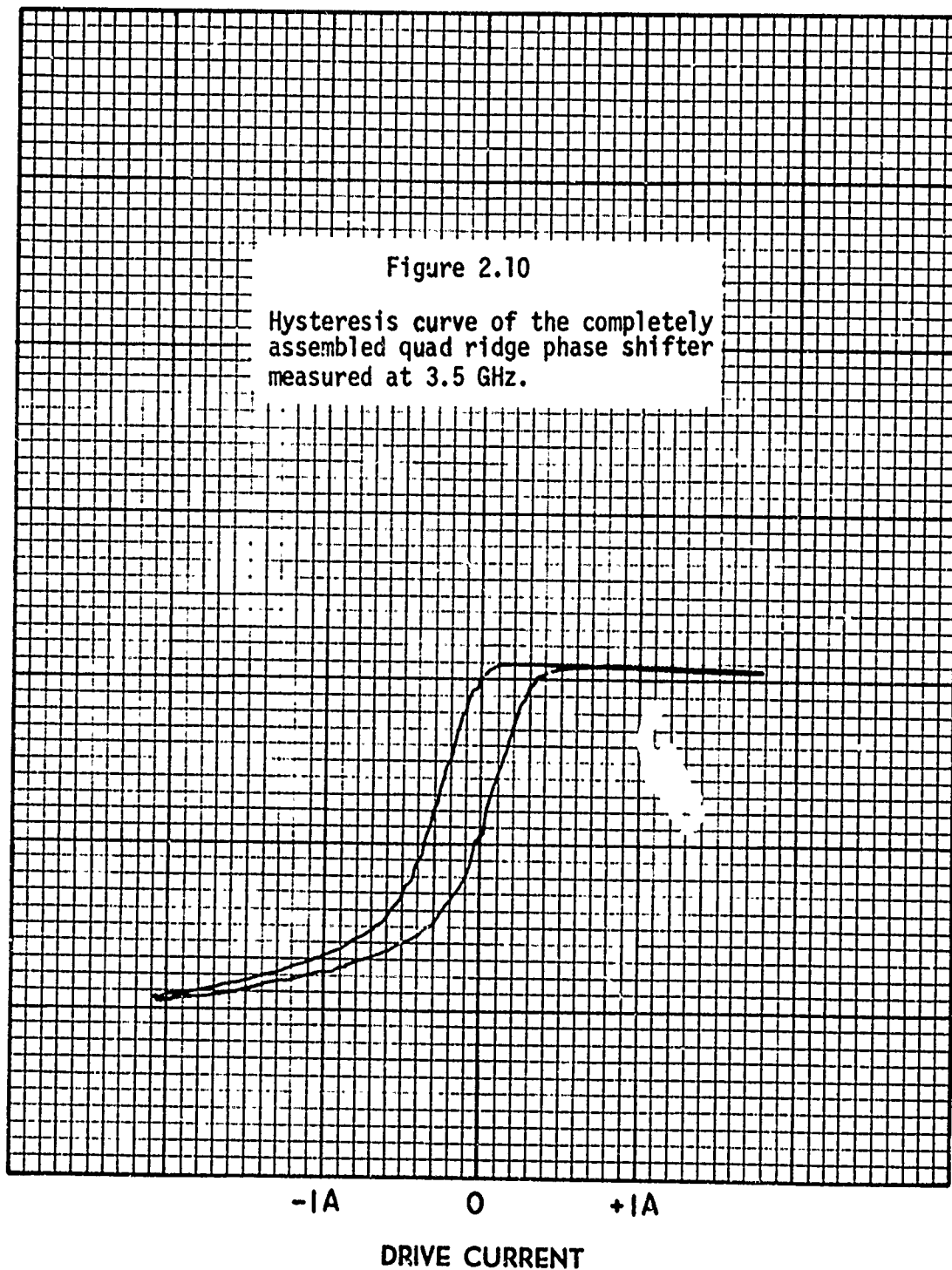
of attributing this loss to reflection effects can be discounted because the return loss remains approximately the same, and consistently belo` . ᴰB. Thus the field increase must be increasing or broadening fe ʳomagnetic ʳesonance, but it is not affecting the waveguide cutoff frequency. l· ɪering the saturation magnetization lowers the saturation resonar e frequency, $\omega_0 = \gamma 4\pi M_s$, upon which the ferromagnetic resonance frequency ω_r depends according to Kittel's equation. Thus by operating at a frequency further above resonance, the increase in resonance frequency due to the application of transverse magnetostatic field will have a lessened effect on insertion loss in the passband of operation. The price one pays for this decreased loss is a less efficient phase shift per unit length.

In addition to altering the saturation magnetization of the material, the length of the transverse magnetostatic interaction area was increased. By increasing the length, a field of lesser magnitude can provide the 90° differential phase delay required for circular polarization. Since the spreading effect of ferromagnetic resonance is quite non-linear, a one-half reduction in field strength will produce far more than one-half reduction in insertion loss.

A new phase shifter was constructed using both of these two loss reduction techniques. Final data is summarized in the graphs of Figures 2.11 to 2.14. In Figures 2.11 and 2.12, families of insertion loss and return loss are shown for extreme latched phase states and five intermediate phase states. The quad ridge geometry can be matched much better than is shown in Figure 2.12. A short 600 Gauss rod that

31

was tested before the final assembly was matched to 15 dB return loss over a 500 MHz bandwidth, but the transformer sections for the short rod did not work as well on the newer longer 600 Gauss rod. The data is sufficiently representative, however, and the base insertion loss of 1.5 dB is expected to be reasonably achievable. The insertion loss drip to 3 dB at 2.9 GHz can be improved by insuring a better match and accurately shielded polarizers.

Figure 2.13 is an important graph showing both phase dispersion as a function of frequency and device reciprocity. This graph was obtained by latching the phase shifter to one extreme of its hysteresis loop and then sweeping the phase variation versus frequency. The linearity of this curve is an indication of insertion phase variation, and the difference between the two curves is an indication of latched phase dispersion. By flipping the garnet rod end-for-end in its test fixture and retaking this data one obtain' the dotted curves, clearly indicating device reciprocity.

The quad-ridge waveguide phase shifter has been clearly shown to be feasible. In the design developed for this program, a 50% reduction in cross-sectional area has been obtained compared to the full height unridged waveguide prototype. Some increase in length was necessary in order to achieve impedance matching to unloaded rectangular waveguide, and also to achieve low loss differential phase sections. Insertion loss is still somewhat higher than an unridged ferrite-loaded waveguide design, but this may still be reduced by improving the design. The quad-ridge phaser design should be of significant advantage in S-band phase shifter application.
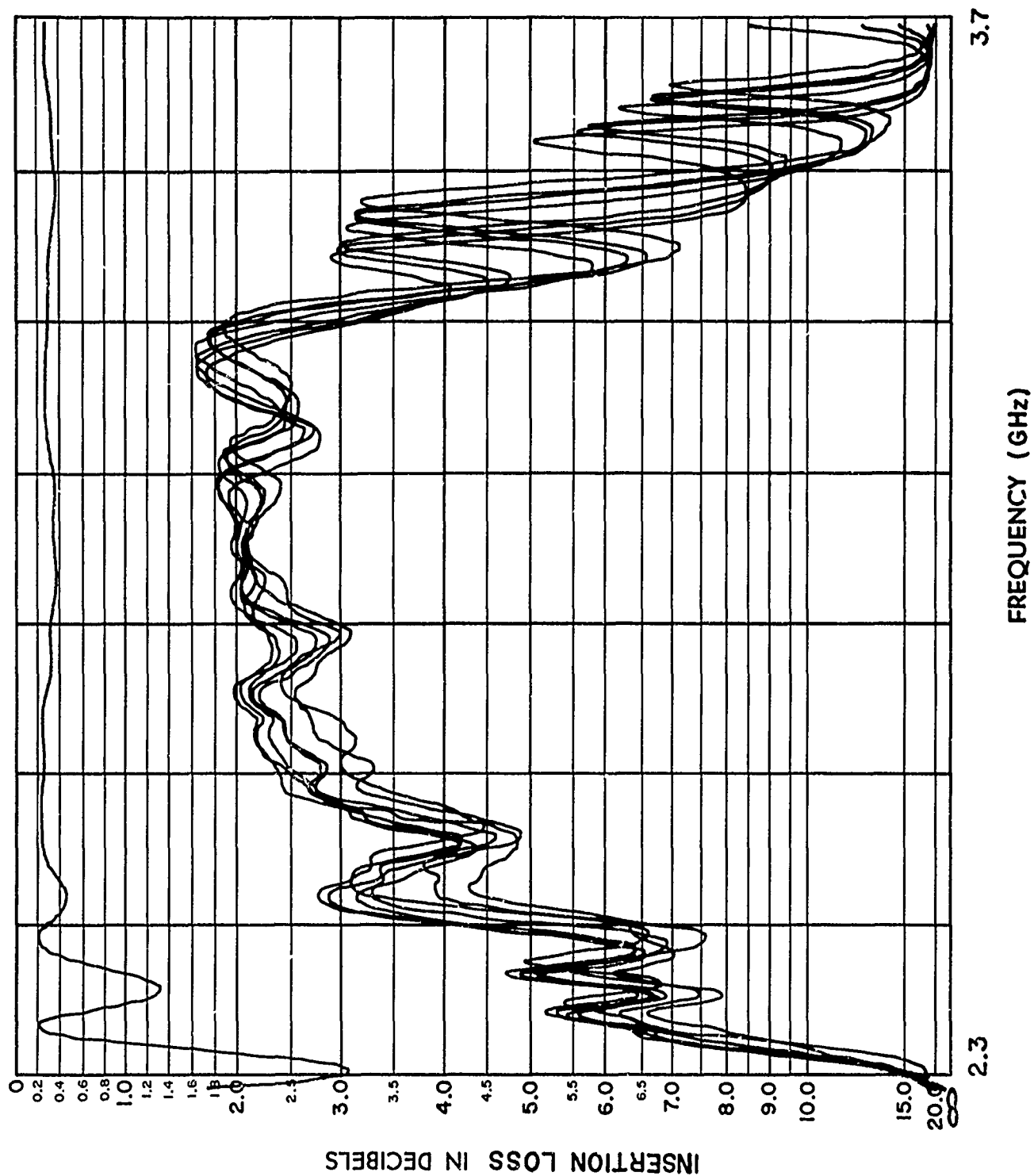
Figure 2.11

Quad ridge phaser insertion loss
for various latched phase states.
Reference 0 dB is at top.

33
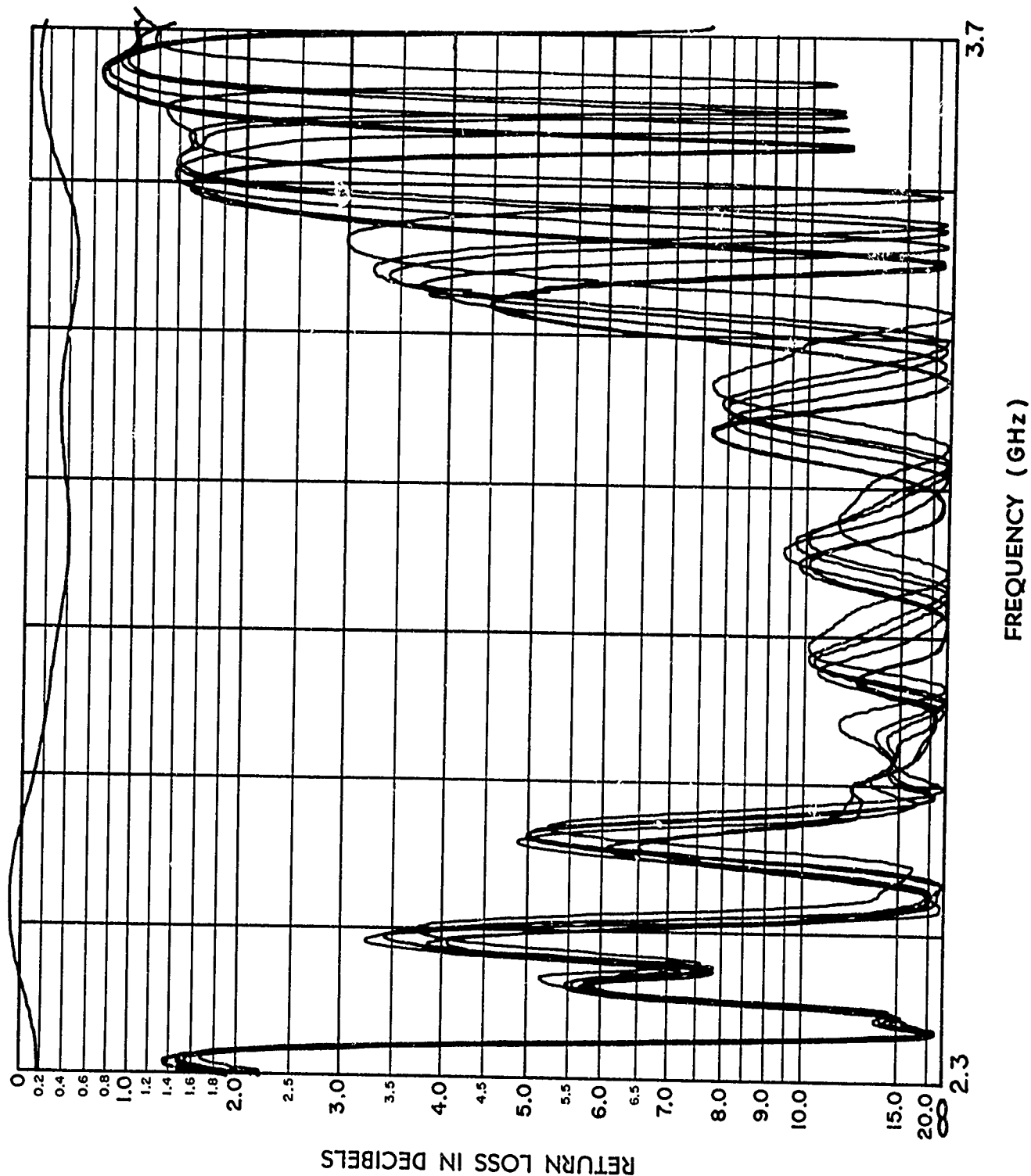
Figure 2.12

Quad ridge phaser return loss for
various latched phase states.
Reference 0 dB is at top.
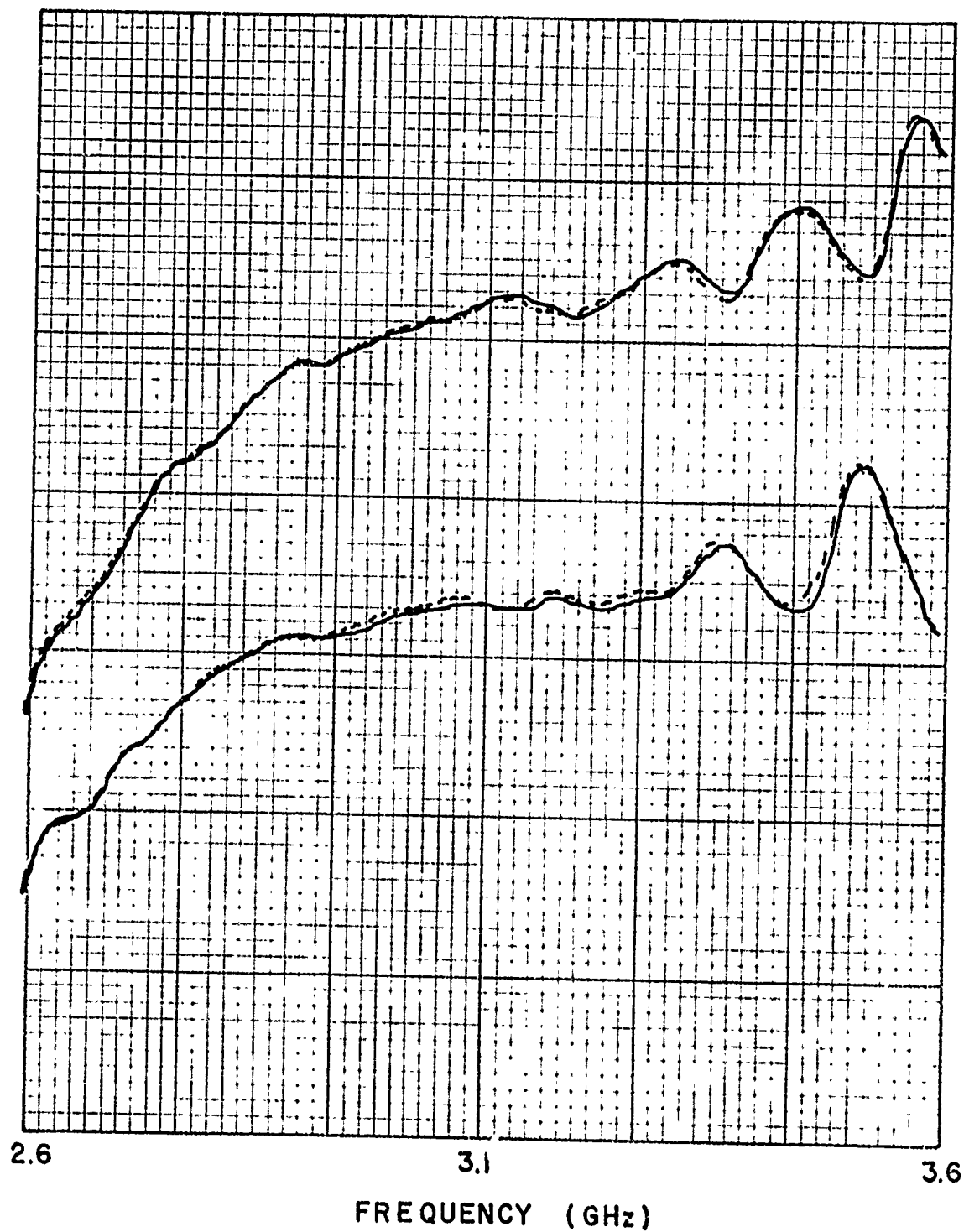
Figure 2.13

Insertion phase of the two extreme latched phase
states. The distance between curves is the
available latched phase of the device. The dotted
curve was taken in reverse position and indicates
reciprocity.

35
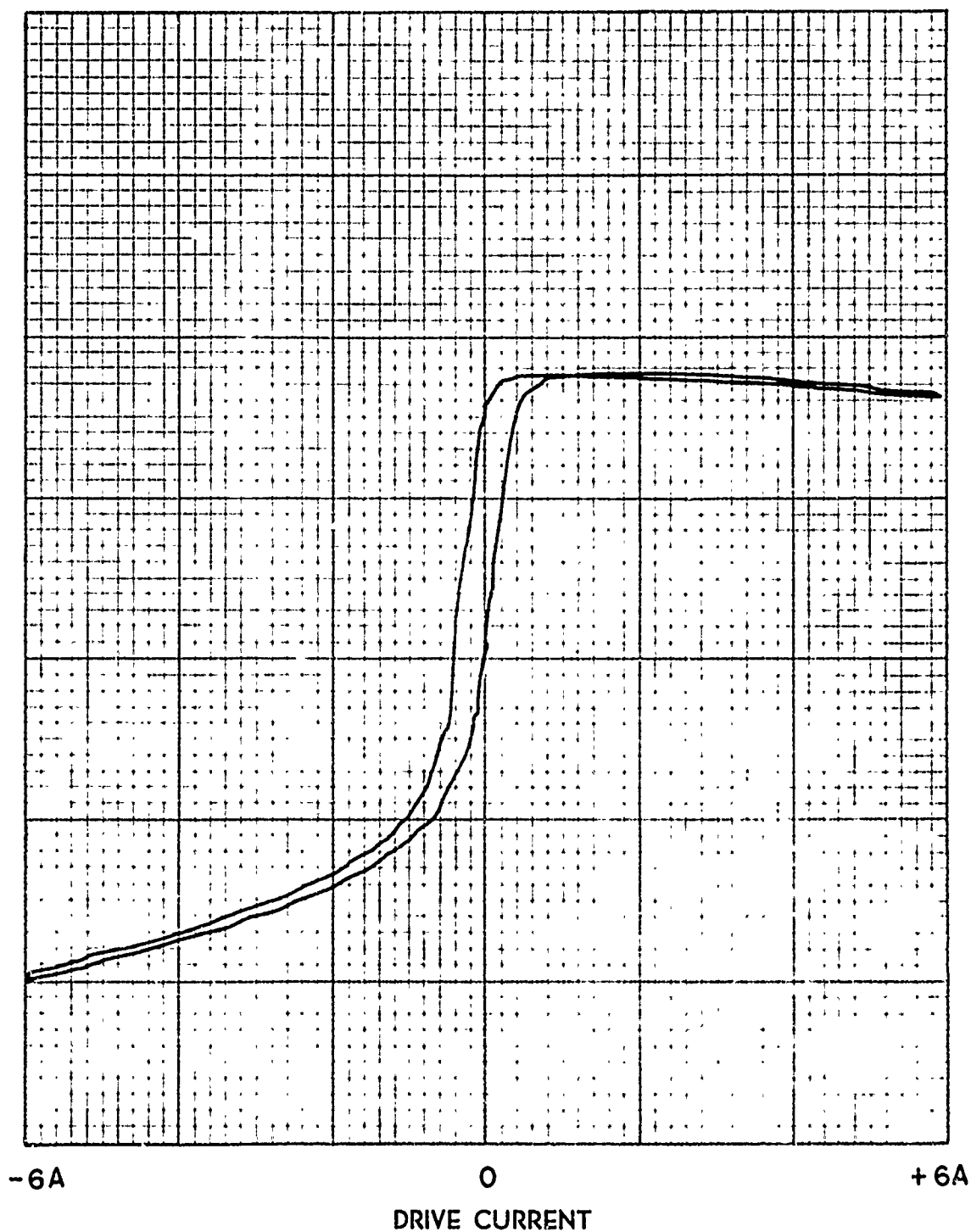
Figure 2.14

Hysteresis curve of the quad ridge phaser
measured at 3.0 GHz. Available latched
phase of the device is determined by the
zero current crossover points.
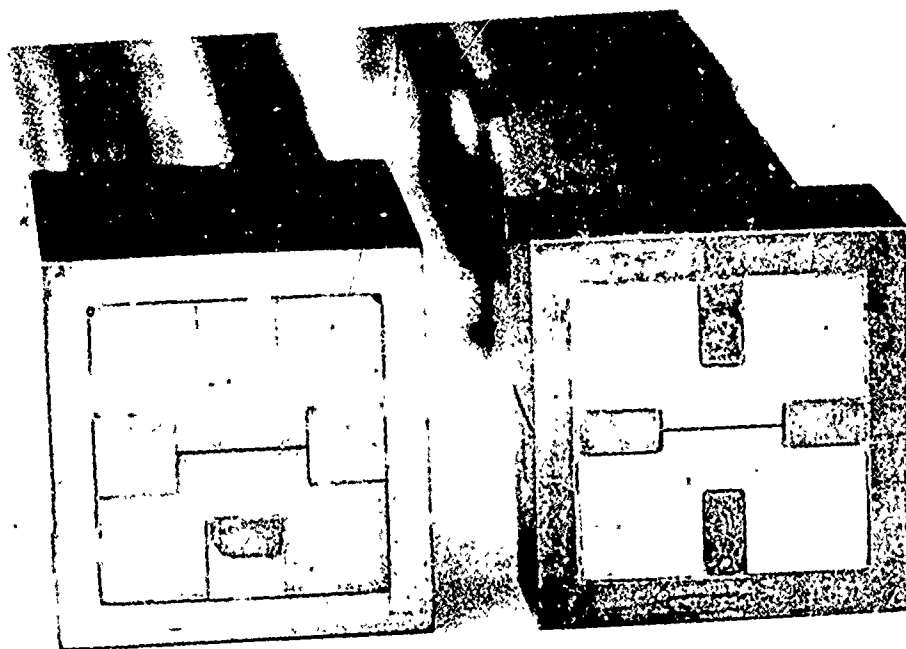
Figure 2.15

End view of the two ridge dimensions investigated
in the quad ridge waveguide designs.
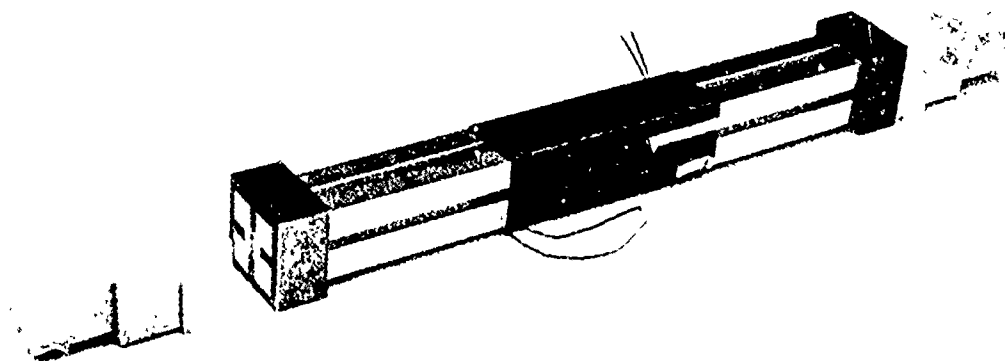
Figure 2.16

Assembly showing quad ridge garnet rod with phase
control coil wound around the center length sections.
Bushings at ends of rod form the interior waveguide
wall and also hold the quad ridge section of the
four section matching transformer.

Figure 2.17

Quad ridge garnet rod in its test fixture.

Figure 2.18

Fully assembled quad-ridge waveguide reciprocal
latching ferrite phase shifter.

38

III

SLOTLINE/MICROSTRIP DUAL MODE PHASER

The slotline/microstrip dual mode phaser owes its operation to a unique propagating structure designed especially for this application and consisting of a sandwich slotline (3) closely coupled by gyro-magnetic medium to a balanced microstrip. A sketch of the interaction r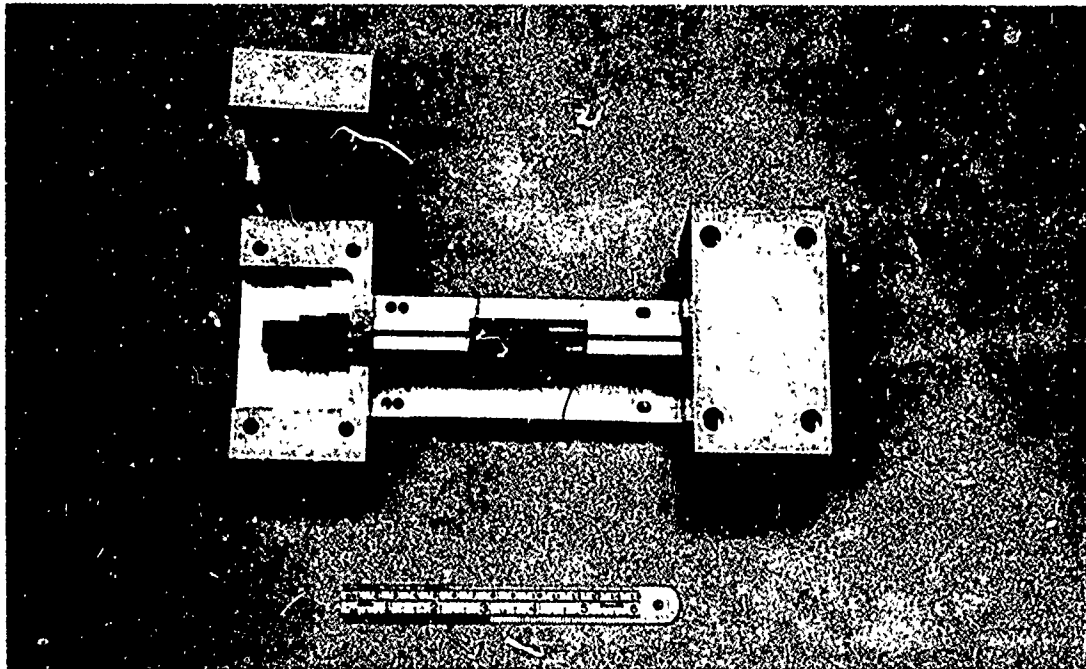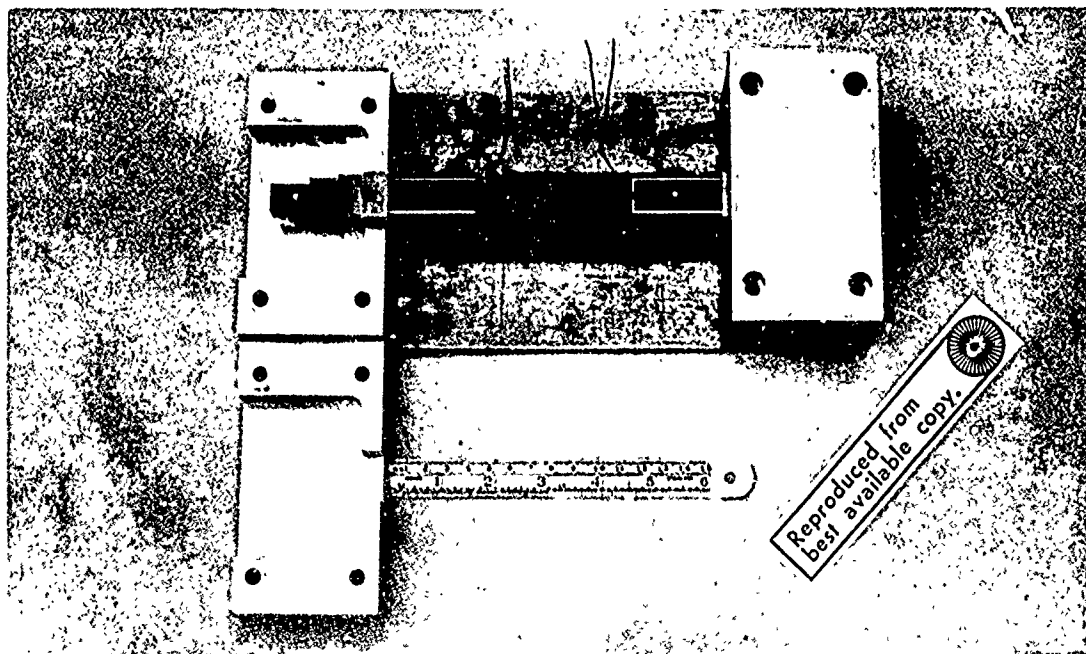egion cross section is shown in Figure 3.1e. From the nature of the geometry and its double reflection symmetry, the medium is seen to be capable of propagating two normal modes.

The two normal modes to which reference will be made are the two lowest order modes. Higher order modes will be excluded by frequency/ geometry design so that the coupling interactions are exclusively restricted. The field configuration of these two normal modes are complex, but similarity to known modes gives a clue to their nature. To begin with there are two principle transmission lines supporting these modes, the slotline transmission line and the microstrip trans-mission line, indicated by (b) and (d) in Figure 3.1. The field configuration for each separately is known. Naturally, when the transmission line types are combined as in Figure 3.1e the field configurations of the composite need not resemble those of the individual components. However, strong arguments exist to imply that they do.
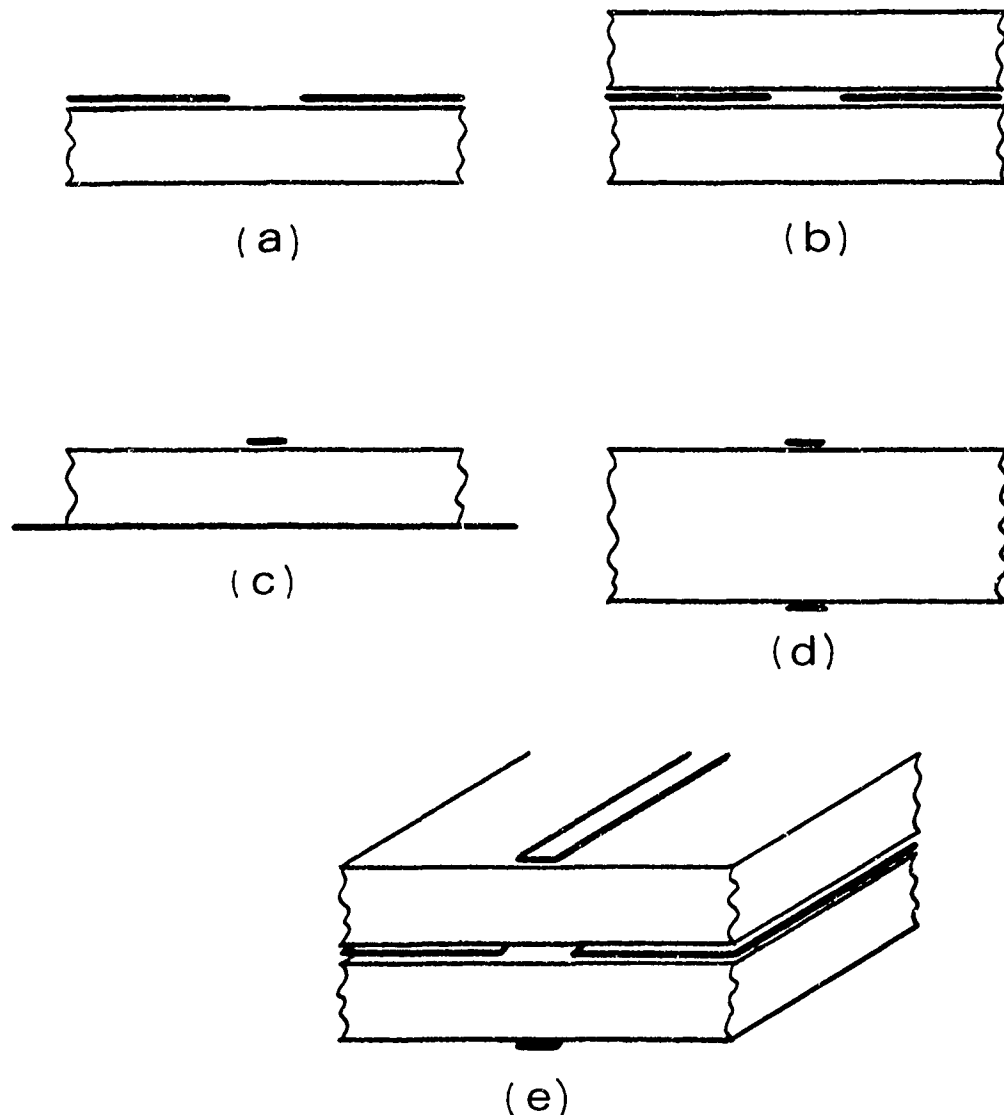
Figure 3.1

(a) Single sided slotline in which a transmission line is formed by the gap in a ground plane deposited on a dielectric substrate.

(b) Sandwich slotline in which a second dielectric slab is added. This adds both symmetry and concentration of the field close to the slot area.

(c) Normal microstrip in which a single conducting strip is deposited on a dielectric slab with a ground plane on the opposite side.

(d) Balanced microstrip in which the strip image as seen through the ground plane physically replaces the ground plane.

(e) Slotline/microstrip composite structure used for the reported phase shifter application.

40

Consider first the balanced microstrip (cf. Figure 3.1b). The field configuration before the addition of the slotline is merely that of a normal microstrip plus its ground plane image. The addition of the slotline conductors will not disturb those fields far from the slot, nor will it disturb them at the center of the slot. At the slot edges it is reasonable to expect fringing fields to concentrate that would otherwise have been evenly distributed, but the effect of this will depend upon the relative widths of slot and microstrip. It can be reasoned, then that by proper selection of conductor widths, the insertion of the slotline ground plane will not seriously affect the propagation characteristics of the microstrip.

The insertion of the microstrip conductors into the field configuration of the slotline is a far more serious matter. Since no change has been made to the air-dielectric interface, the dominant mode may be expected to remain TE. However, electric field lines that might hitherto have been parallel to the slab face above the slot area must become perpendicular in order to satisfy the equipotential boundary conditions on the microstrip conductor. The corresponding effect on the phase velocity is impossible to predict. To evaluate this, then, a sequence of tests was initiated to compare the guide wavelength of the 2 conductor slotline-only transmission line with the 4 conductor slotline/microstrip transmission line. The results are recorded in Appendix B and surprisingly indicate no significant difference between the two. This result is important to the subsequent investigations because it suggests that tests and manipulations

41

of the slotline alone will indicate the behavior of the 4 conductor normal mode after addition of a microstrip conductor.

To simplify identification, the uncoupled normal mode having an electric field component parallel to the slotline plane at the central symmetry axis will be designated the slotline mode, and the uncoupled normal mode having an electric field component perpendicular to this plane will be designated the microstrip mode. Phase shifter suitability tests (1) have indicated that each such mode is bound to its respective transmission line and furthermore that they may be mutually coupled by the gyromagnetic ferrite medium. These same phase shifter suitability tests indicated a 99% coupling capability for appropriate design. Implementation into a complete phase shifter, having been shown to be practical and promising, was the next sequential step.

The principle features of a reciprocal ferrite dual mode phase shifter have already been described in the introduction. A slotline/microstrip version is slightly more complicated due to the requirements of a microstrip launch into the slotline, and a resultant block diagram would appear as shown in Figure 3.2. The reciprocity is indicated by the arrows at either end. The 3 dB dividers are achieved by longitudinal magnetization. The 90° differential phase sections, which will be discussed in considerable detail shortly, are achieved by shorted slot stubs. And the central phase control section is achieved by latched longitudinal magnetostatic flux drive.
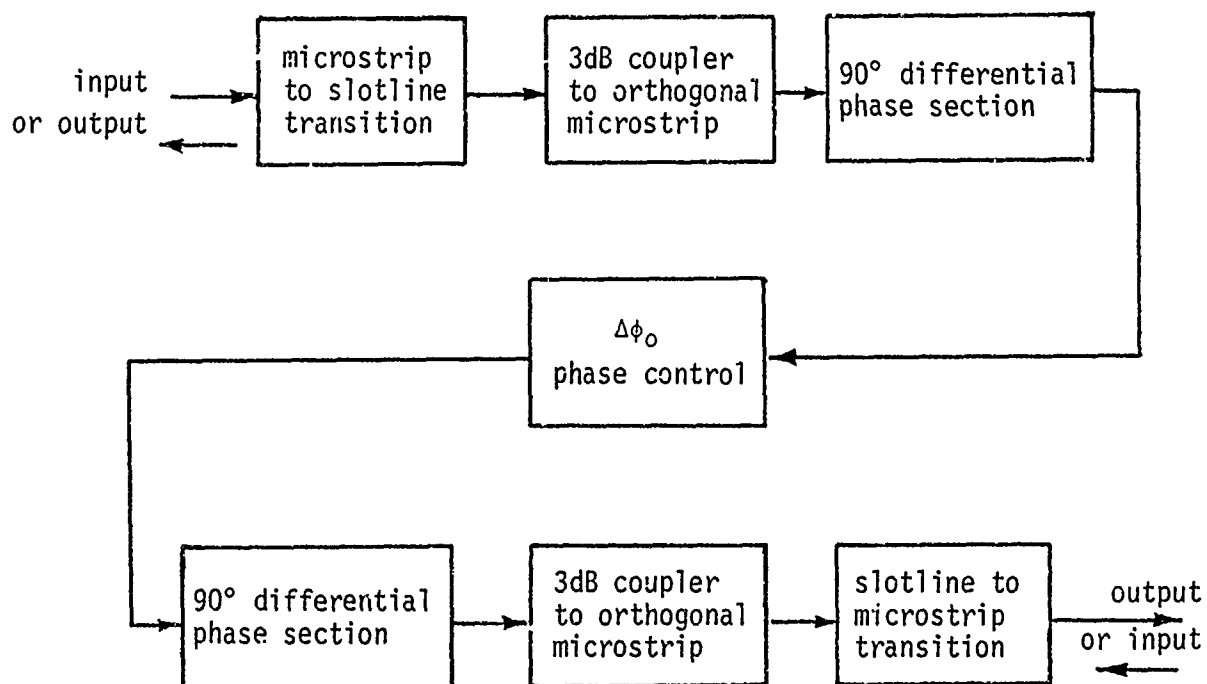
42

Figure 3.2

Symbolic block diagram of a complete phase
shifter using the composite slotline/
microstrip transmission structure.

43

The principle difficulties in assembling a phase shifter with this overall design were twofold. First, the mechanical difficulty of providing coil slots without severing critical sections of the ground plane, and second, the 90° differential phase sections. The present solution to the former problem is depicted without further elaboration in Figure 3.3. The 90° differential phase section difficulties require further discussion.

The purpose of the differential phase section is to delay one of the modes relative to its mate by 90°. Since the 3 dB dividers have split the input slotline energy equally between the slotline and microstrip modes, a 90° delay of either will generate a new modal relationship commonly known as circular polarization. The sense of this newly induced CP will depend upon which mode was delayed by 90°.

There are four types of transverse magnetization schemes possible for the 90° differential phase sections. Sketches of each are shown in Figure 3.4. Schemes (A) and (C) have potential application by delay of the slotline mode relative to the microstrip mode. In fact, a number of authors have heralded slotline as a promising new phase shifter medium because of the expected potential phase delay with just such a geometry. Each of these schemes proved a dismal failure. Only when the magnetization became so strong that the flux spread through the length and beyond the 3/4 inch magnetic area could the phase delay reach as high as 50°/inch. It was concluded that the quantitative results of these tests were

Figure 3.3

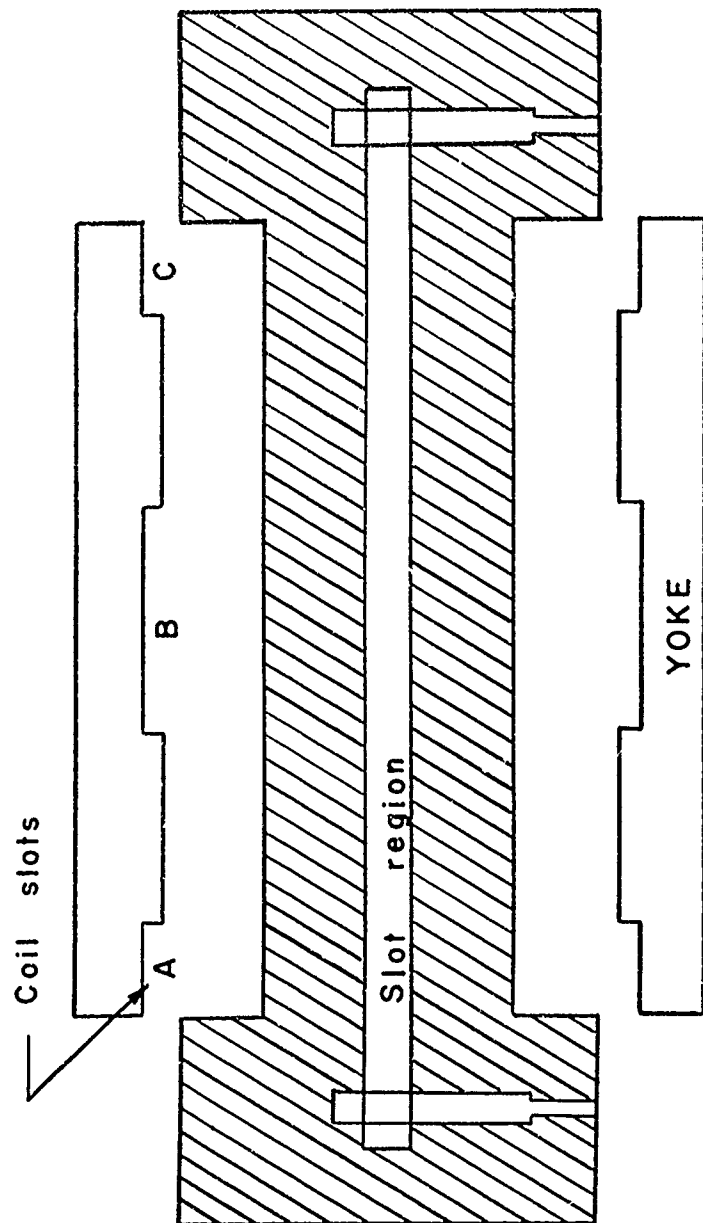Sketch of the garnet slab layout showing partitioning of the yoke sections relative to the slotline. In this configuration the coil may be wound around the center garnet region without slicing the input ground plane of the microstrip launch.
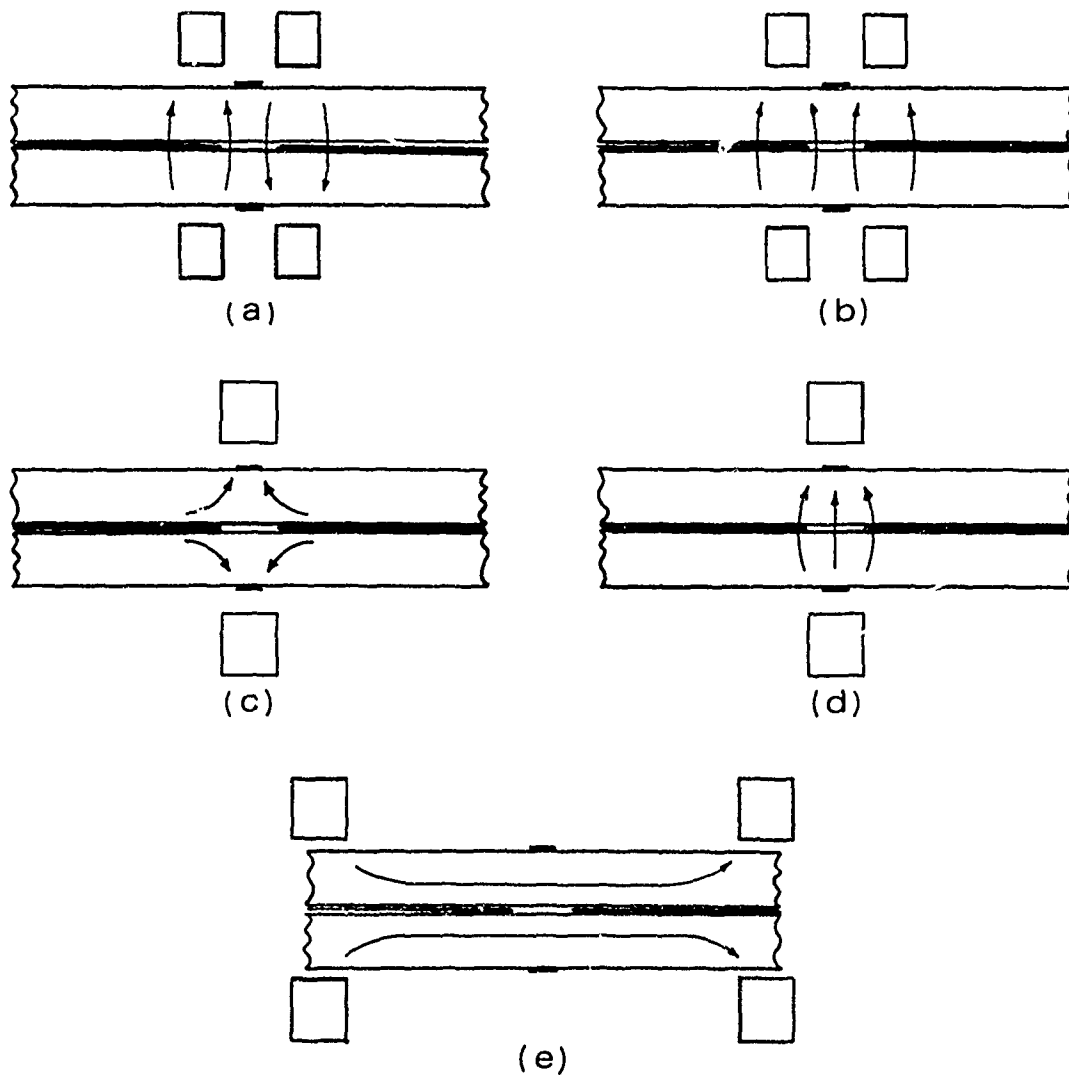
Figure 3.4

Cross sectional views of the slotline/microstrip
interaction area showing transverse magnetization
techniques employed to achieve 90° differential
phase shift.

invalid because their relative effectiveness depended more upon ability to magnetize external regions of ferrite than upon the shape of the magnetostatic field in the desired interaction area. Qualitatively it was concluded that proposed phase shifter schemes using slotline only would not produce sufficient figures of merit to become commercially viable phase shifters.

After these various magnetization schemes, two _physical_ delay techniques were employed. The first of these, the "meander line" technique shown in Figure 3.5, induced sharp discontinuity reflections very similar to those encountered in the phaser suitability tests of the semi-annual report. This scheme was quickly superceded by the slot stub scheme shown in Figure 3.6. The equivalent circuit is shown in Figure 3.6b. Each stub in a set of six acts as a series impedance to the slotline transmission line, indicated in the equivalent circuit by the characteristic impedance Z_0. Each of the 3 pairs of shorted slotline stubs acts upon the slotline as a lumped reactance on the slotline transmission line. The condition for match requires that when the output is terminated in an impedance Z_0, the impedance seen at the input is also Z_0. Hence

$$Z_0 = Z_1 + Z_a \frac{(Z_2 + Z_m) \cos \theta_a + j Z_a \sin \theta_a}{Z_a \cos \theta_a + j (Z_2 + Z_m) \sin \theta_a}$$

where

$$Z_m \equiv Z_b \frac{(Z_3 + Z_0) \cos \theta_b + j Z_b \sin \theta_b}{Z_b \cos \theta_b + j (Z_3 + Z_0) \sin \theta_b}$$

47
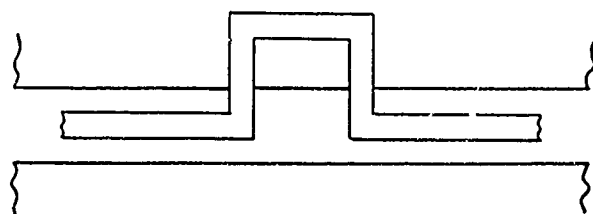
Figure 3.5

Sketch of the "meander" modal delay technique
in which the balanced microstrip conductors
are brought outside the slotline area.

(a)
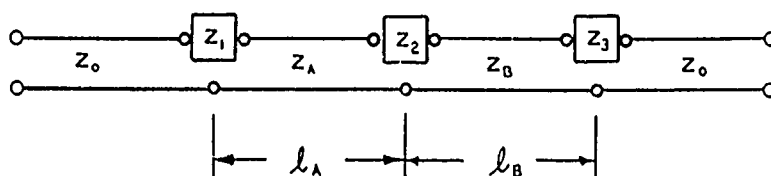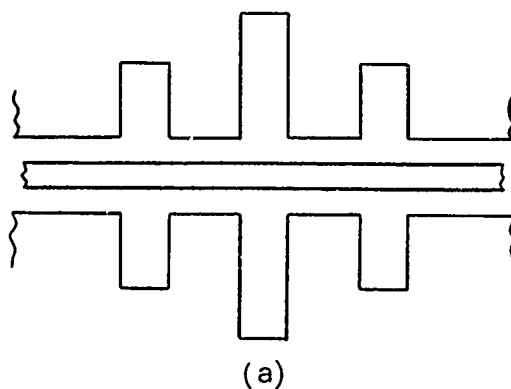
Figure 3.6

Sketch of the slot-stub delay technique. In
this sketch, the outline of the slotline formed
by ground plane deposit on a garnet substrate
is shown with the balanced microstrip conductor
positioned in the center for reference. The
slot outline is distorted by the addition of
shorted stubs of orthogonal slotline. Each
may be considered as a lumped series impedance
to the transmission line equivalent circuit
shown in (B).

48

Electrical length $\theta_a = \beta_a \ell_a$ and $\theta_b = \beta_b \ell_b$. For a reciprocal phase delay network there are restrictions on the parameters. For reciprocity,

$$Z_1 = Z_3$$

$$Z_a = Z_b$$

$$\theta_a = \theta_b \equiv \theta$$

This simplifies the condition for match considerably, and if all impedance variables are normalized to Z_a then this condition may be written as follows.

$$\sin^2\theta \; (x_1^2 x_2 - z_0^2 x_2 + 2x_1) - \cos^2\theta \; (2x_1 + x_2)$$
$$+ \sin\theta \cos\theta \; (2x_1 x_2 + 2x_1^2 - 2z_0^2 - 2) = 0$$

Where, by definition,

$$x_1 \equiv X_1/Z_a \quad \text{and} \quad jX_1 \equiv Z_1$$

$$x_2 \equiv X_2/Z_a \quad \text{and} \quad jX_2 \equiv Z_2$$

$$z_0 \equiv Z_0/Z_a$$

Lastly, for quarter wavelength separation, $\theta = \beta\ell = \pi/2$ and the condition required for match simplifies to
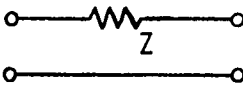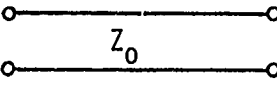
$$\frac{x_1}{x_2} \; (x_1 x_2 + 2) = z_0^2 \qquad\qquad [3.1]$$

The next step is to determine the condition required to achieve the desired 90° differential phase shift. Utilizing ABCD matrices defined by

49

$$V_1 = AV_2 - BI_2$$

$$I_1 = CV_2 - DI_2$$

it is easily determined that the appropriate matrices for a series impedance, shunt admittance, and transmission line segment is

Fundamental Element	ABCD Matrix
Z	$\begin{bmatrix} 1 & Z \\ 0 & 1 \end{bmatrix}$
Y	$\begin{bmatrix} 1 & 0 \\ Y & 1 \end{bmatrix}$
Z_0	$\begin{bmatrix} \cosh \gamma\ell & Z_0 \sinh \gamma\ell \\ Y_0\sinh \gamma\ell & \cosh \gamma\ell \end{bmatrix}$

The composite ABCD matrix of the triple stub section is then

$$\begin{bmatrix} A & B \\ C & D \end{bmatrix} = \begin{bmatrix} 1 & Z_1 \\ 0 & 1 \end{bmatrix} * \begin{bmatrix} \cos\theta_a & Z_a\sin\theta_a \\ Z_a^{-1}\sin\theta_a & \cos\theta_a \end{bmatrix} *$$

$$* \begin{bmatrix} 1 & Z_2 \\ 0 & 1 \end{bmatrix} * \begin{bmatrix} \cos\theta_b & Z_b\sin\theta_b \\ Z_b^{-1}\sin\theta_b & \cos\theta_b \end{bmatrix} * \begin{bmatrix} 1 & Z_3 \\ 0 & 1 \end{bmatrix}$$

The asterisk symbol is used to signify matrix multiplication. Now, to find the insertion phase, specify that the triple stub section be terminated in the characteristic impedance of the external transmission line so that $V_2/(-I_2)=Z_0$. Using the ABCD definition equations the insertion ratio V_1/V_2 may quickly be determined to be

50

$$\frac{V_1}{V_2} = A + B/Z_0$$

After collecting A and B from the matrix multiplication and making
the appropriate reciprocity simplifications

$$\frac{V_1}{V_2} = 1 + K_1 \sin^2\theta + K_2\cos^2\theta + K_3\sin\theta\cos\theta$$

with

$$K_1 = -\frac{jX_1^2 X_2}{Z_0 Z_a^2} + \frac{j2X_1}{Z_0} - \frac{X_1 X_2}{Z_a^2}$$

$$K_2 = +\frac{j2X_1}{Z_0} + \frac{jX_2}{Z_0}$$

$$K_3 = \frac{j2X_1}{Z_a} + \frac{jX_2}{Z_a} + \frac{2Z_a}{Z_0} - \frac{2X_1 X_2}{Z_a Z_0} - \frac{2X_1^2}{Z_a Z_0}$$

The insertion phase ϕ is

$$\phi = \tan^{-1} \frac{I_m \{V_1/V_2\}}{R_e \{V_1/V_2\}}$$

As with the match condition equation, if each length section is
made a quarter wavelength, $\ell_a = \ell_b = \lambda/4$ then $\theta = \beta\ell = \pi/2$ and

$$\phi = \tan^{-1} \frac{-\dfrac{X_1^2 X_2}{Z_a^2 Z_0} + \dfrac{2X_1}{Z_0}}{1 - \dfrac{X_1 X_2}{Z_a^2}}$$

A differential phase of 90° requires the stub loaded line to have
an additional 90° delay over an unloaded line running the same
length. If the characteristics of the internal sections of the

51

line between stubs has not been altered then the overall length is
a half wavelength for the unloaded line as well as the loaded line
and

$$\phi = \frac{\pi}{2} + 2\beta\ell = 3\pi/2$$

The condition required for proper phase is then

$$X_1 X_2 = Z_a^2 \qquad\qquad [3.2]$$

Combining the two equations specifying the condition for match [3.1]
and the condition for 90° differential phase [3.2] it can be determined
that

$$X_1 = Z_0/\sqrt{3}$$

$$X_2 = \sqrt{3}\ Z_a^2/Z_0$$

Since the series reactances will be introduced by series sections
of shorted slotline (cf. Figure 3.6), then for each such section
(n=1,2)

$$Z_n = jX_n = jZ_{0n} \tan \beta_n \ell_n$$

To create a design from this information, one may freely specify
the characteristic impedance Z_{0n} of the nth shorted stub. Since Z_0
is dependent upon the W/D ratio of the slotline, and since the slab
thickness D is fixed, this is equivalent to selecting the slotline
width W. Selecting a width W = .094 inch and using corrected values
of β_n led to a design as shown in Figure 3.7. Each stub is inter-
preted to constitute a lumped series impedance physically located at
the stub centerline, hence symmetric stubs on opposing sides of the

52

slotline are considered to be in series. The insertion loss of the slotline with stubs in place is shown in Figure 3.8 and the insertion phase for various configurations is shown in Figure 3.9. Comparison of curves A to C and C to E in Figure 3.9 indicate that the two delay networks were not identical, for their insertion phases differ by about 25% throughout the frequency band. The discrepancy is apparently due to slight variations in the assembly process and was certainly unexpected. The discontinuities for the two unsymmetrical configurations, B and D, is due to radiation of normally evanescent modes which are suppressed in the symmetrical configurations. The sharp attenuation after 3 GHz in Figure 3.8 was not able to be removed and is thought to be due to an inopportune choice of slot stub width (.094 inch). Previous studies noted in the Semi-Annual Report showed that the minimum W/D ratio to avoid surface wave mode radiation effects at S-band was W/D $\cong$ 1.5. Since greater thicknesses are desirable to maximize the percentage concentration of energy into the gyromagnetic medium this effectively limits the slotline width to a minimum of 1.5D just as it previously limited the substrate thickness to a maximum of 0.67W. Thus, for the fixed substrate thickness W should be maintained at .187 inch. In any event the phase delay networks performed satisfactorily over the 24% bandwidth from 2.5 to 3.1 GHz, and the reciprocal system phaser properties could be assessed.

Results of the tests are shown in Figures 3.10 to 3.12. Reference to Figure 3.11 indicates a latching phase range of about 40°. Since this
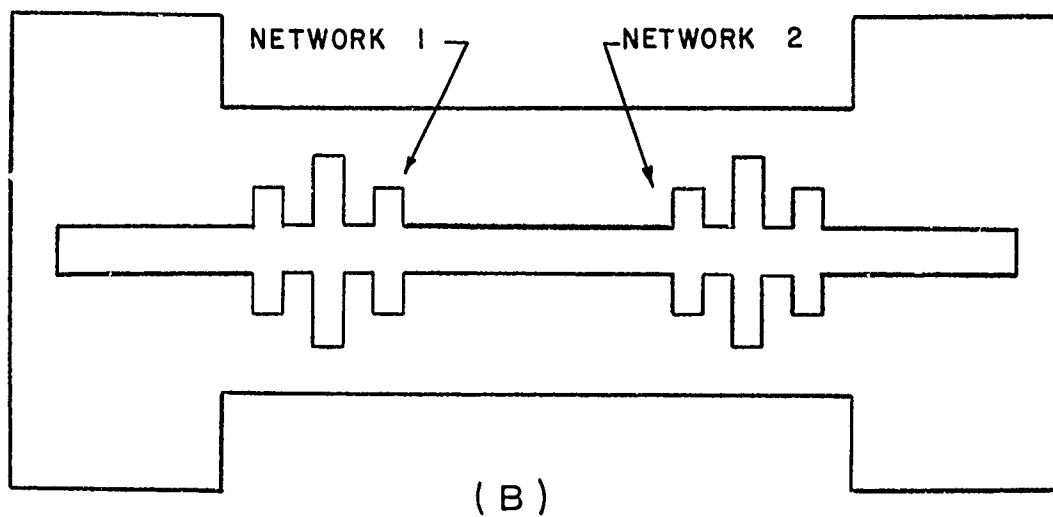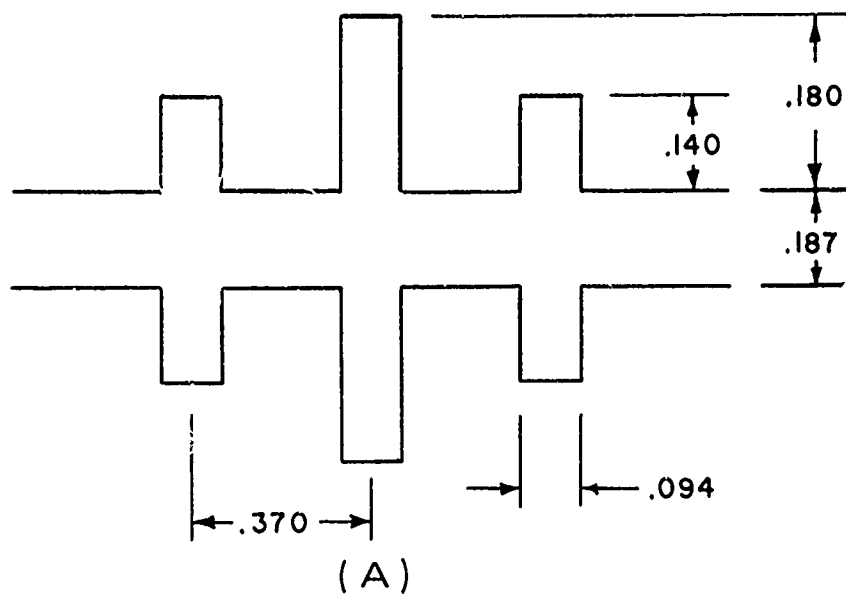
Figure 3.7

Slotline stub dimensions for 90° differential phase
sections on sandwich slotline with X805 garnet sub-
strate material, each slab .125 inch thick. Sketch
(B) shows placement of the two delay networks on the
6 X 2 inch garnet slab.
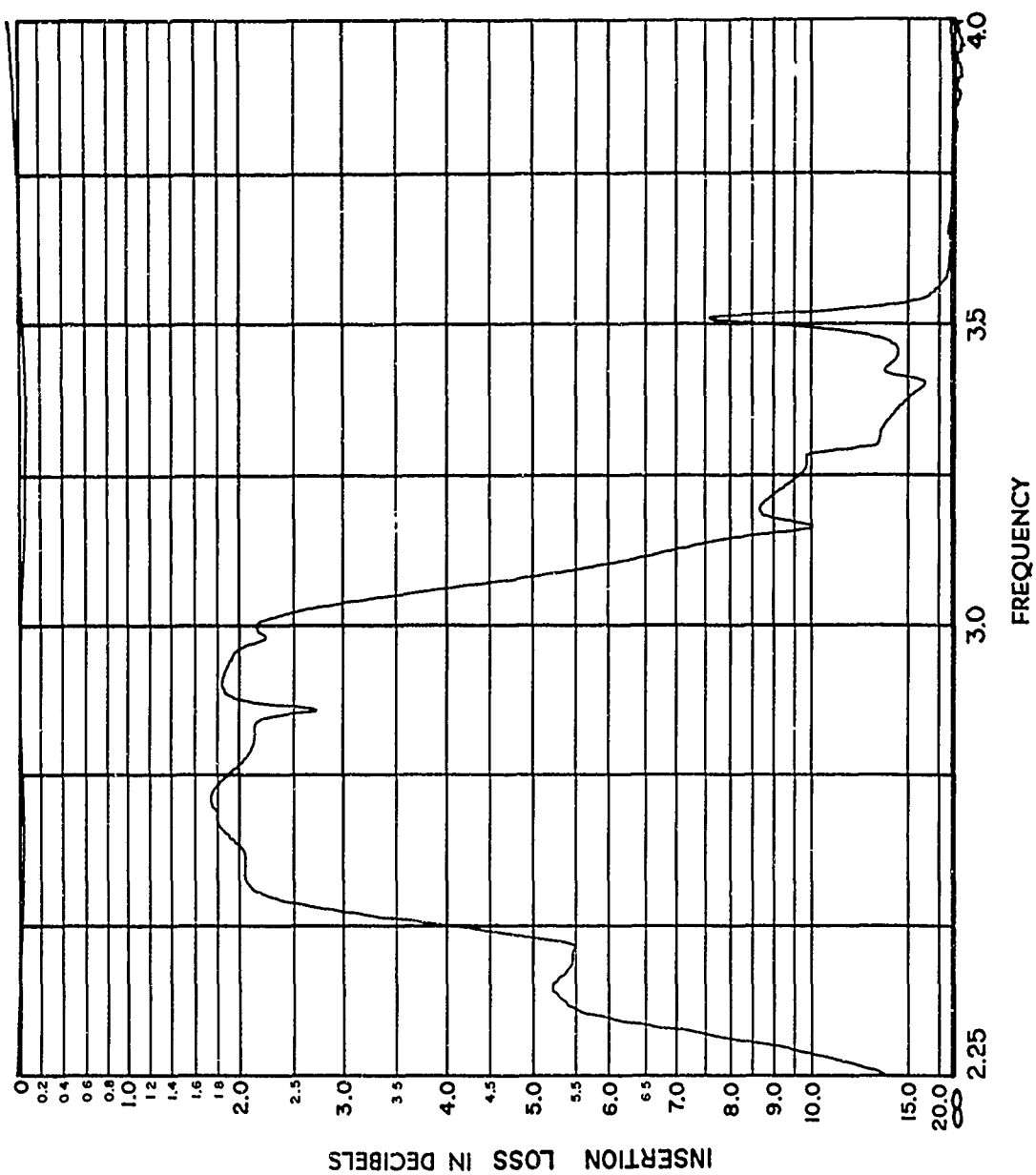
Figure 3.8

Insertion loss of slotline after loading with the
shorted slot-stub sections for differential phase
delay. Prior to loading bandwidth extended to
about 3.7 GHz.

55
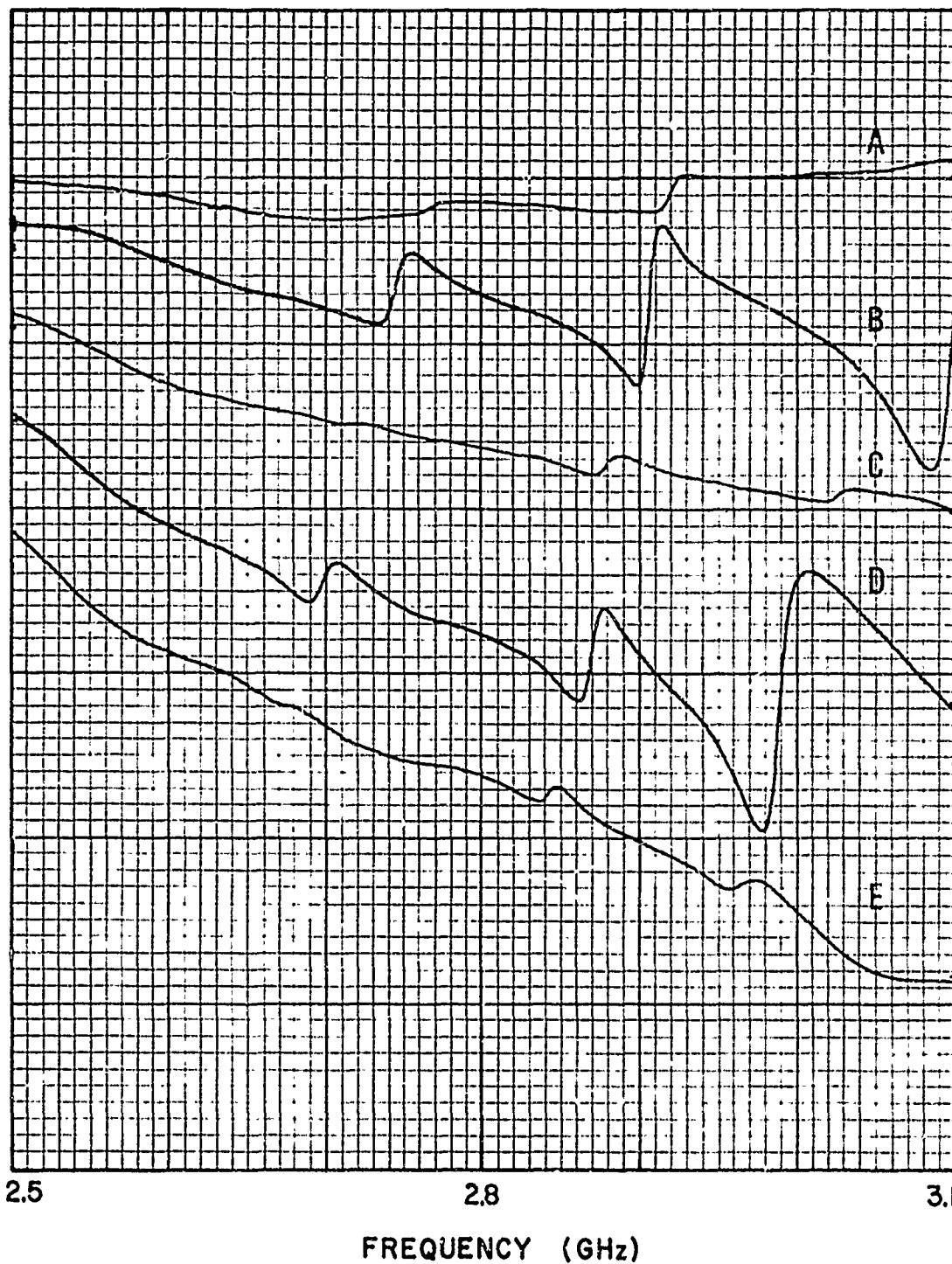
Figure 3.9

Phase delay of slotline with various levels of slot-stub loading.
(A) Slotline only
(B) Slotline with one 3 stub section
(C) Slotline with two 3 stub sections
(D) Slotline with three 3 stub sections
(E) Slotline with all four 3 stub sections
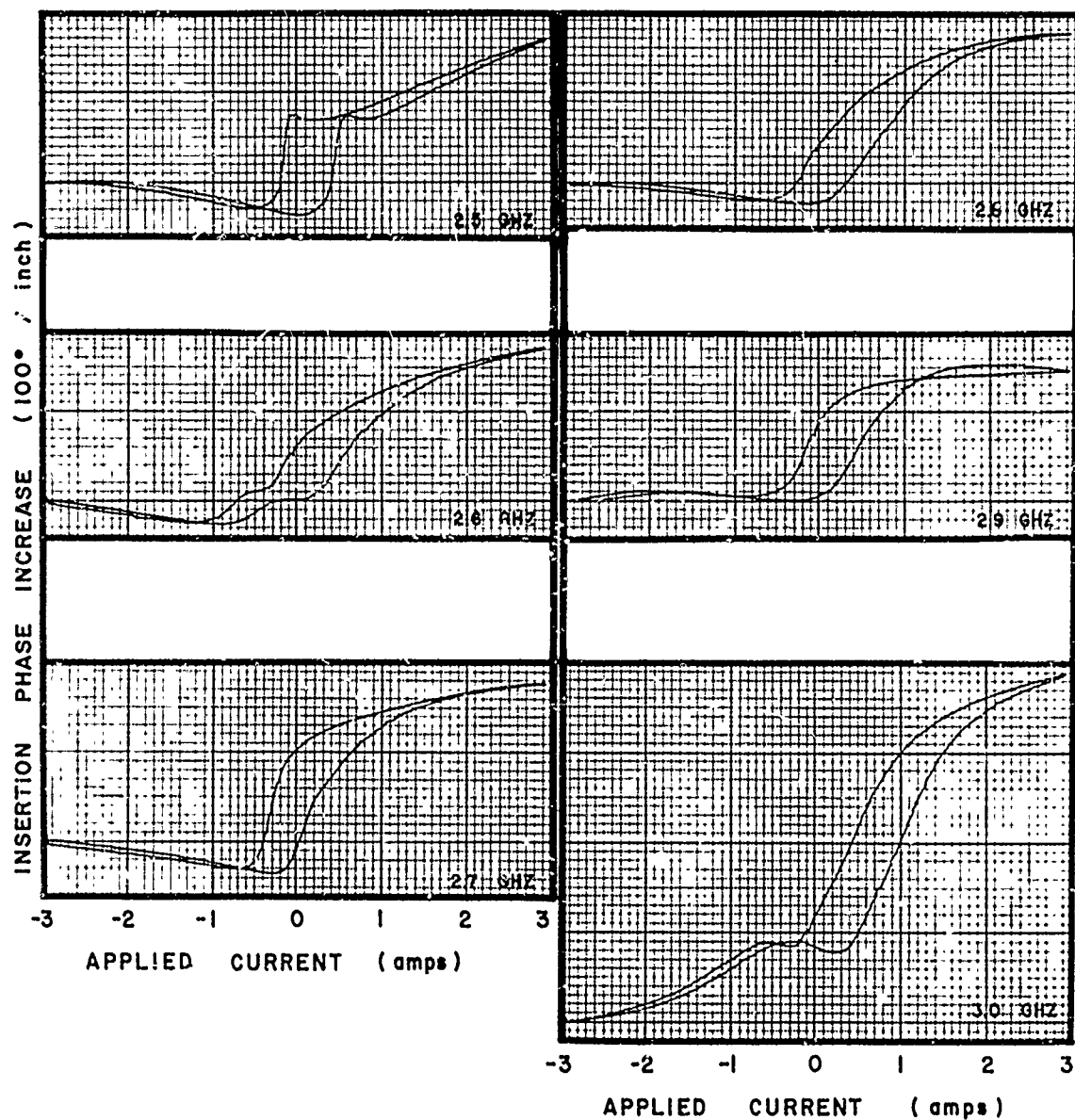
Figure 3.10

Hysteresis plots for the slotline/microstrip phase
shifter at various frequencies. Available latched
phase shift can be determined from the zero current
crossover points. Asymmetry is due principally to
longitudinal field bias interaction.

57
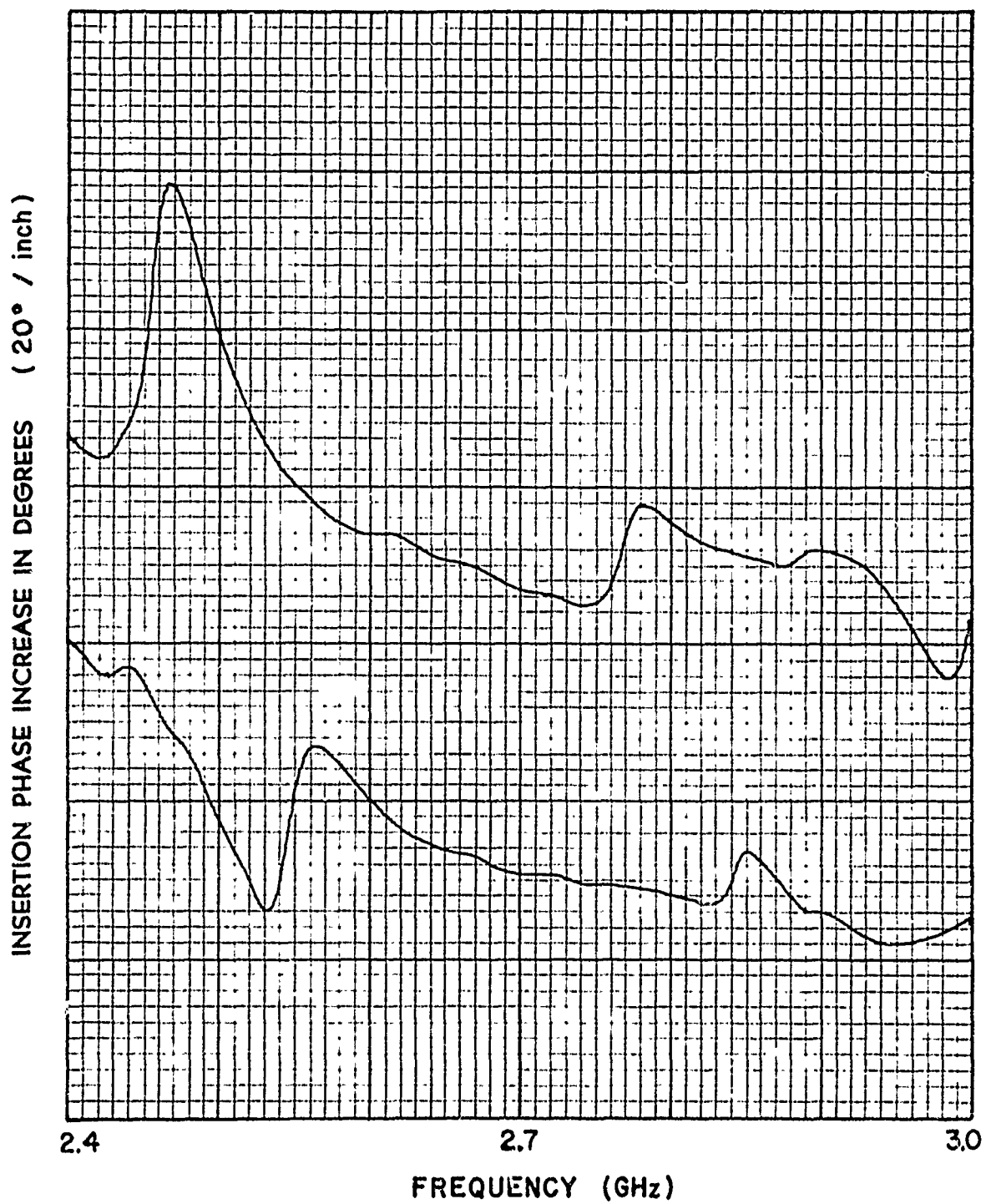
Figure 3.11

Swept trace of the latching phase states, SET state above and RESET state below, for the slotline/microstrip phaser with constant 1A in 3 dB orthogonal coupler coils.
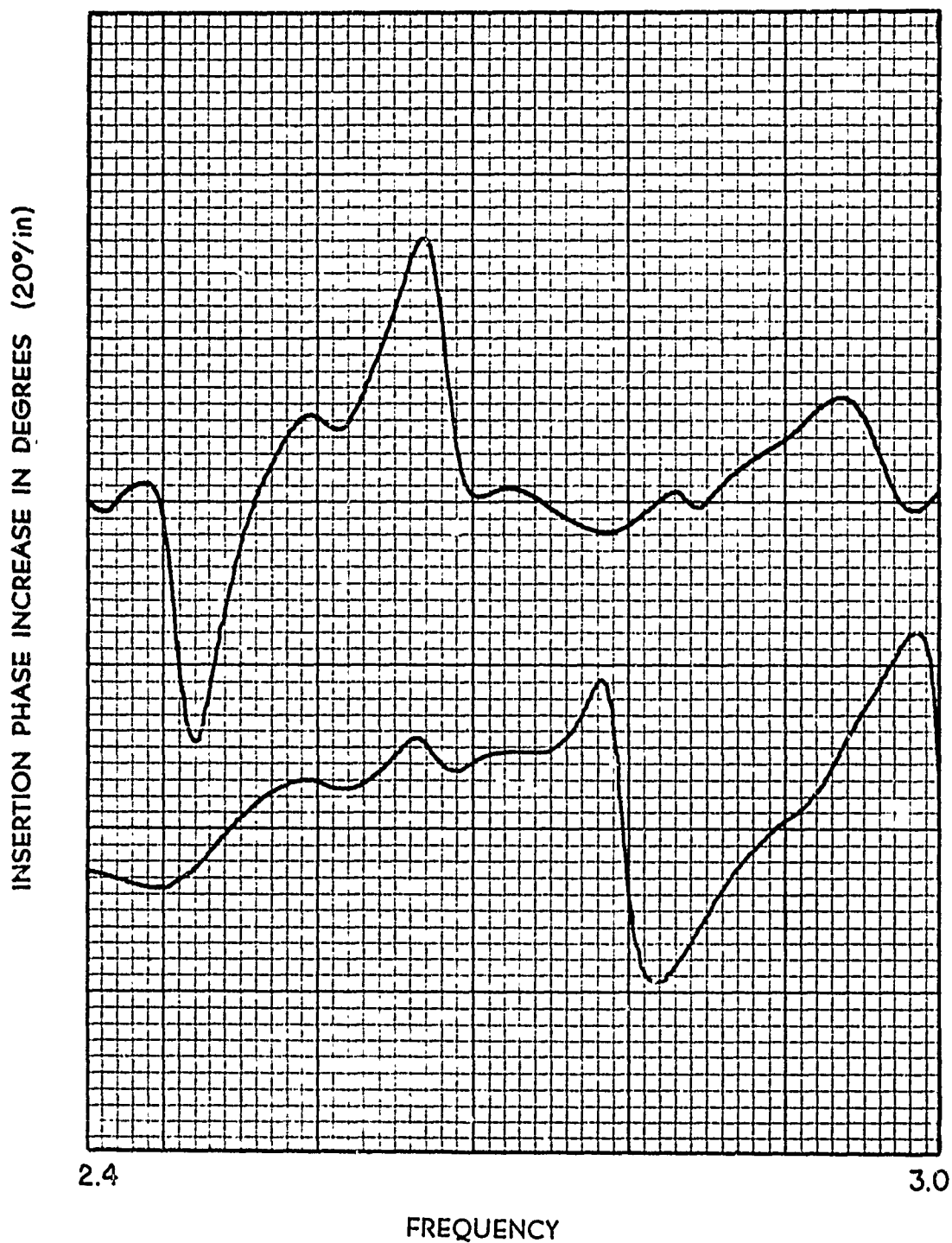
Figure 3.12

Swept trace of latching phase states for the slotline/microstrip
phaser with 3 dB division coil replaced by Indox V permanent magnet.

was achieved with a 5/8 inch long coil, which is a very small inter-
action length, the phase capability may be said to be 64°/inch. The
asymmetry of the hysteresis curves of Figure 3.10 is due to long-
itudinal field interaction. There are three longitudinal field sections,
and of these the two 3 dB division fields are oriented similarly
while the central $\Delta\phi$ phase control fields varies in direction and
amplitude. A sketch of the relative directions of these three fields
is shown in Figure 3.13. The three arrows represent magnetostatic
field directions for the 3 longitudinal field sections in approximately
the same relative positions as they would appear to an observer looking
down on the broad face of the garnet slab.

Relative magnetostatic field directions of
latched RESET state

Relative magnetostatic field directions of
latched SET state
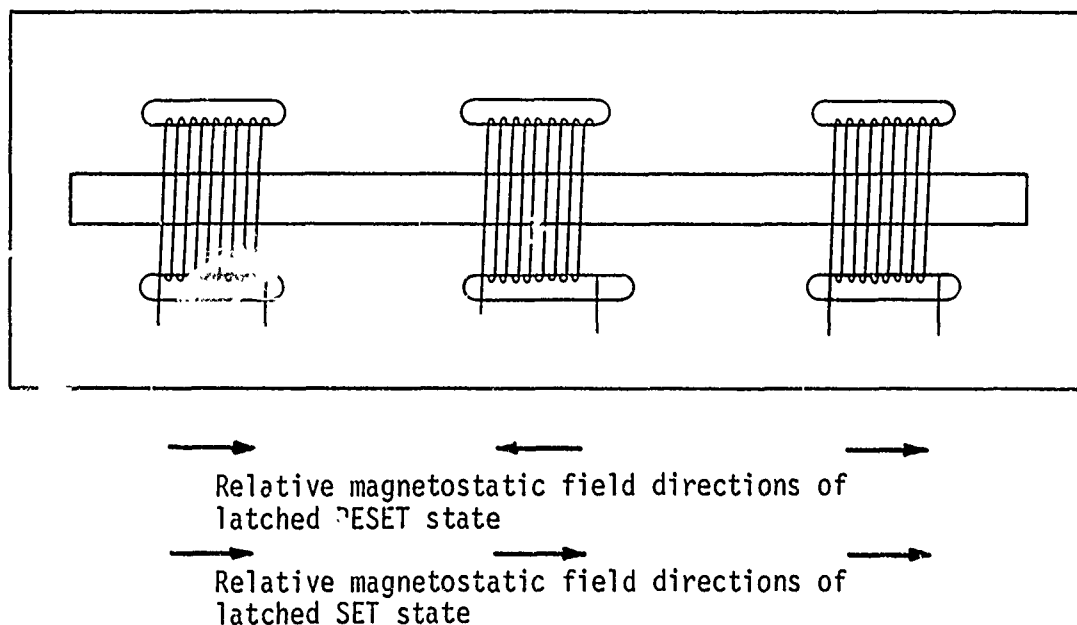
Figure 3.13

Relative field directions for the two
extremes of phase control bias. The
three coils whose fields are represented
are sketched above.

60

When the three fields are aligned, the net effective interaction length of each is increased. For the central phase control section this merely increases the available phase, but for the 3 dB division networks the effect is to distort the circular polarization into elliptical polarization of variable eccentricity.

This concentration of flux phenomenon also has a bearing on the available phase of a given design. A short section of phase control length will not have as much net <u>longitudinal</u> field as a longer section, and for very short sections the net proportion of the field which is actually longitudinal may be very small indeed. Figure 3.14 demonstrates this phenomenon. The effect is not dissimilar to the alignment phenomenon mentioned earlier.

SHORT COIL

LONG COIL
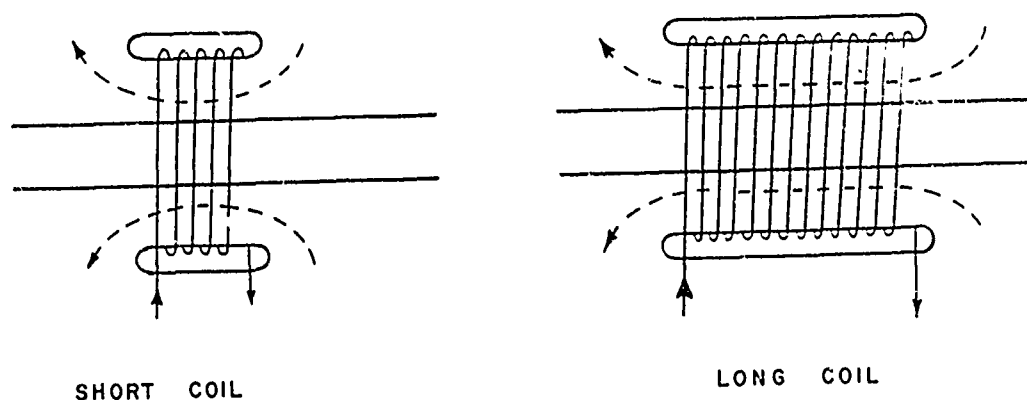
Figure 3.14

Sketch of magnetic fields, shown as dotted lines,
and how they would appear for different length coils.

Using this same sketch it is easy to visualize a curling of the magnetic field close to the slot when faced with a nearly opposing field, whereas if the two adjacent fields of Figure 3.12 are in similar alignment there will be a tendency to form a new flux path enclosing both slots thereby increasing considerably the net percentage of magnetic field in the longitudinal direction. The present point, however, is the available phase of a given design and its relation to bhe phase control coil length. Very small coil lengths will lower the effectiveness of a design. It is estimated that the observed phase availability of 64°/inch could be increased to 100°/inch given the benefit of added length. A figure of merit can be estimated assuming that the 2 dB insertion loss is linearly related to length. The present 5/8 inch coil length would increase to 3.6 inches, and the overall 7 inch length would increase to 9.98 inches; the present 2 dB insertion loss would increase to 2.85 dB and the estimated figure of merit becomes 126°/dB.

This slotline/microstrip phase shifter design shows considerable promise for reciprocal, latching, ferrite phase shifter applications at S-band frequencies. With the crossed microstrip-to-slotline excitation technique this design should interface easily with microstrip power distribution schemes. Furthermore, due to the planar geometry and deposited conductors, this phaser design is expected to be very low cost, especially in production quantities.
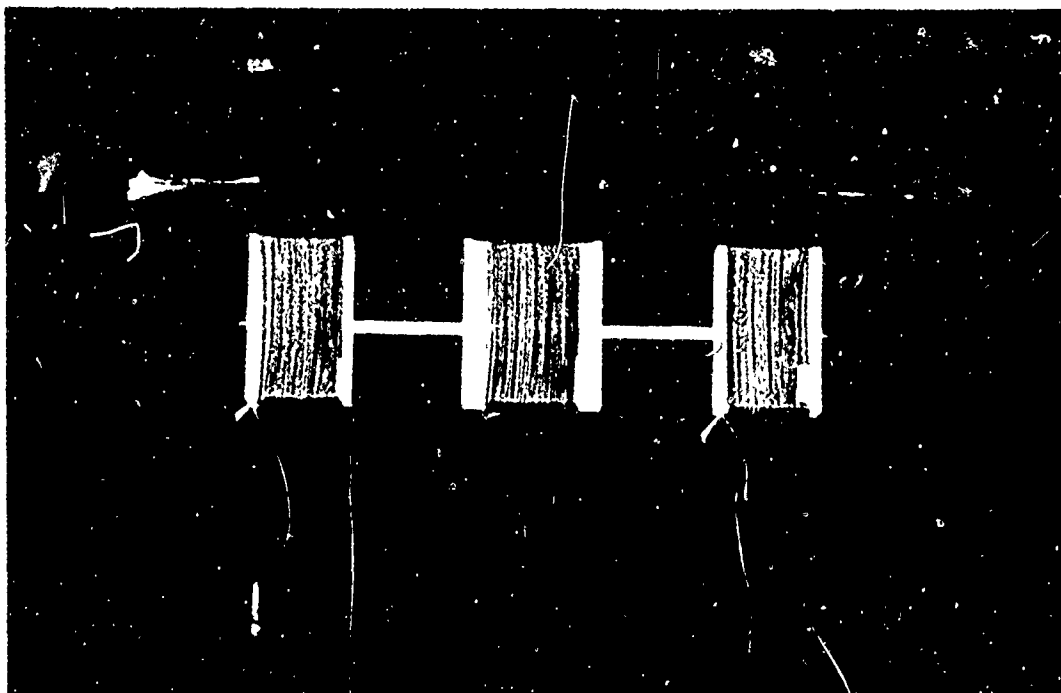
Figure 3.15

Garnet substrate of the slotline/microstrip phaser
showing construction technique and placement of
the three coils.
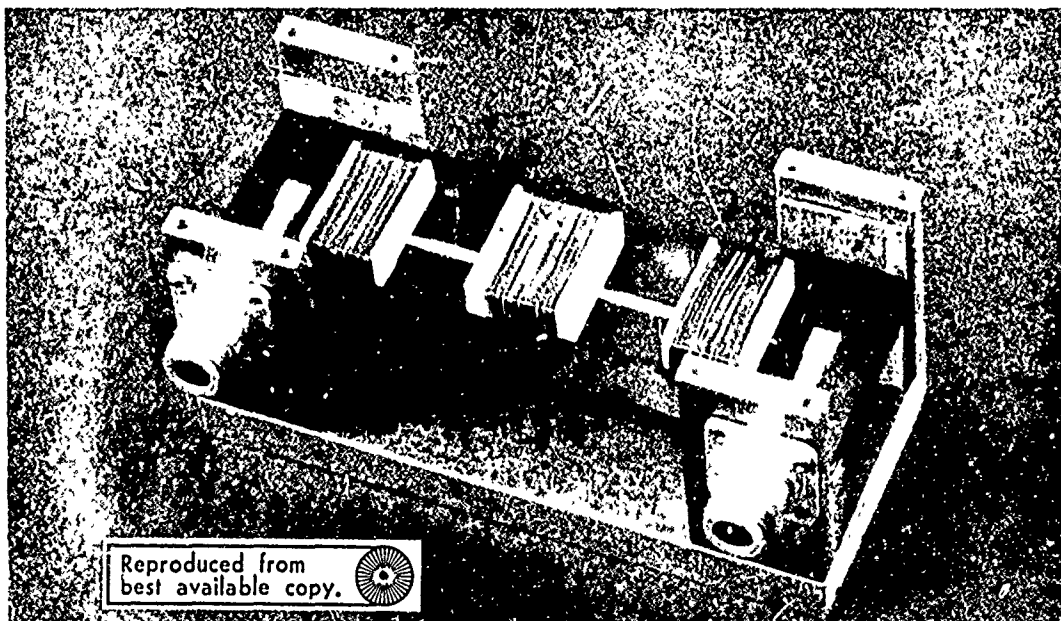
Figure 3.16

Slotline/microstrip phase shifter in its housing
showing the coax to microstrip launch and the
microstrip to slotline launch.
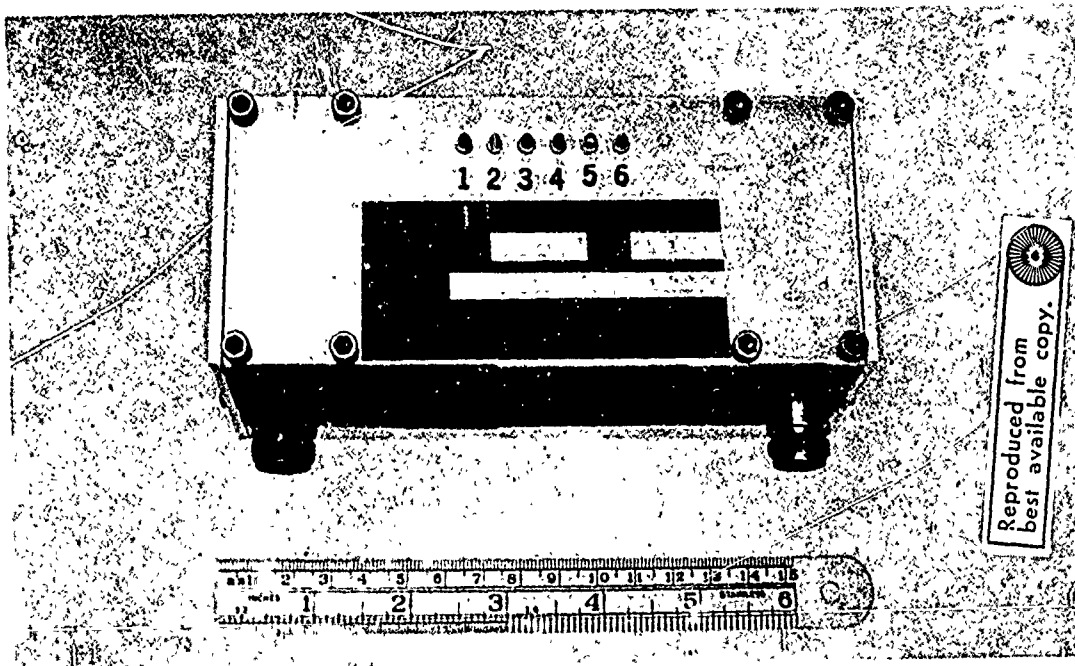
Figure 3.17

Photograph of the complete phase shifter assembly.

IV

SUMMARY AND CONCLUSIONS

Two promising types of reciprocal latched phase shifters have been brought to the developmental prototype stage. Each employs a dual mode principle in which contra-rotating senses of circular polarization are subjected to controlled phase delay for opposing directions of propagation.

The first phase shifter employed a quad ridge waveguide geometry. In this geometry a waveguide region fully filled with ferrimagnetic material is modified by the introduction of ridges. To maintain the symmetry required of a dual mode design, the ridges must be located with double reflection symmetry and thus four equally spaced ridges are required for the waveguide perimeter. The use of ridge waveguide allows for the possibility of reducing cutoff frequency for fixed outside dimensions, or conversely, reducing outside dimensions for a fixed cutoff frequency. The principle impetus for the present design was reduction in size for operation at S-band frequencies.

The desired reduction was effected and a 50% reduction in cross section area was achieved. With G800 garnet interior, a standard design of unridged waveguide requires .8593 in^2 area while the quad ridge design required .4225 in^2. Insertion loss in the new design is higher but phase shift per unit interaction length increased. Launching circular polarization in a quad ridge geometry is now difficult,

65

due principally to a concentration of the CP region susceptible to transverse magnetization. The final geometry of the quad ridge structure had a square outer periphery, 0.650 inch on a side. Two ridge sizes were investigated, 0.172 wide by 0.178 deep, and 0.100 wide by 0.190 deep. Two ferrimagnetic materials were investigated having 800 Gauss and 600 Gauss magnetization.

The wide ridge design was discarded early as it unexpectedly produced unusually high insertion loss. When match to 15 dB return loss the insertion loss of the unmagnetized waveguide section was 6 dB. With the narrower .100 wide ridge structure a similar match produced about 1.5 dB insertion loss. In the first narrow ridge design, an 800 Gauss garnet was used as the ferrimagnetic region, and it was discovered that the magnetic loss due to application of the transverse magnetostatic field required for circular polarization increased considerably. With sufficient field for 90° differential phase delay between orthogonal modes, insertion loss increased to 10 dB or greater throughout the pass band. To offset this effect, a new structure was made from 600 Gauss material and the transverse interaction area length was increased. The resultant phase shifter had a latch phase shift of 100° over the frequency band from 2.9 to 3.3 GHz. Reciprocity was excellent. The insertion loss base value was 1.5 dB. Of the total 10.5 inch length from transformer tip to tip, 2.3 inches were relegated to the interaction length, so that the phase efficiency was 43°/inch. Figure of merit at

66

center frequency 3.1 GHz, based on 100° latched phase shift was 66.7°/dB. Since peak to peak phase shift was 180°, some improvement in squareness should yet be possible. The bandwidth could be improved also, for the match of the final G600 rod was not optimized before phase measurements were made.

The second phase shifter employed a new and unique propagating structure consisting of slotline and microstrip components in a balanced design with double reflection symmetry. A ferrimagnetic material (800 Gauss) formed the substrate upon which the conducting surfaces were deposited. The excitation of energy into the medium required three transition regions on either side, coax to microstrip, microstrip to slotline, and slotline to four conductor slotline/ microstrip. The microstrip to slotline launch was achieved using a crossed slot-strip transition matched to one octave, while the slotline to composite slotline/microstrip transmission line was achieved using a tapered balanced microstrip. Both of these transitions were described in the semi-annual report (1).

To utilize the medium for dual mode operation, phase velocities of the two orthogonal dominant modes must be identical. Mathematically, the normal modes must have degenerate eigenvalues. Using proper choices of conductor geometry this was verified and demonstrated over half octave bandwidths (1). Furthermore, it is necessary to launch circular polarization into the dual mode region to make use

67

of phase control on the normal mode of the medium. This was achieved by a slot stub loading effect to phase delay the slotline mode 90° relative to the microstrip mode. This phase delay network was unexpectedly narrow band, ostensibly due to an inappropriate choice of slot width.

The completed phaser had a latching phase range of only about 40°. This was achieved with a 5/8 inch long interaction area, the remainder of the six inch long slab being required for transition regions and launch of circular polarization. Base loss for the phase shifter was about 2 dB over the range of frequencies from 2.5 to 3.0 GHz. Extension of the upper frequency limit should be possible with an improved slot stub delay network design. The high insertion loss of 2 dB seems to be due in part to the open nature of the propagating medium. Even after replacing the X805 garnet substrate with low loss K15 dielectric material the insertion loss of the 7 inch path length (including all transitions) was a nominal 0.9 dB. One garnet substrate, identical conductor geometry led to a nominal 1.8 dB insertion loss. It is expected that improvements in base loss and bandwidth are possible and that a figure of merit of 126°/dB is a reasonable expectation for this phaser design.

Each of the two phase shifter designs that have been developed under this program offer potential benefits to the microwave designer. The small cross section profile of the quad ridge design offers

reduction in weight and bulk of material as well as the obvious size. Bandwidth of the operation has also been significantly increased over the unridged waveguide prototype. The slotline/microstrip design is the more revolutionary of the two desings, and it offers potential benefits as well. The slotline/microstrip design could prove to have the broadest bandwidths yet achieved in any dual mode phase shifter design. Although only 500 MHz has been verified thus far, the half octave bandwidth from 2.5 to 3.5 GHz seems readily obtainable, and full octave bandwidths require further improvements in transition technology. Perhaps the greatest potential benefit of the new slotline/microstrip design is one of cost. It is expected that the planar geometry and ease of adaptation to microstrip power distribution networks makes this one of the least-expensive reciprocal latching ferrite phase shifter designs available today.

BIBLIOGRAPHY

(1) C. R. Boyd and R. A. Gaspari, "Microwave Reciprocal Latching
     Ferrite Phase Shifters," Semi-Annual Report, Contract DAAB07-
     71-C-0112, Microwave Applications Group, Chatsworth, Calif.

(2) H. N Chait and N. G. Sakiotis, "Broadband Ferrite Rotators
     Using Quadruply Ridged Circular Waveguide," Trans. IEEE,
     Vol. MTT-7, pp. 38-41, January 1959.

(3) S. B. Cohn, "Slotline on a Dielectric Substrate," Trans. IEEE,
     Vol. MTT-17, pp. 768-778, October 1969. A more extensive listing
     of literature related to slotline will be found in the semi-
     annual report, reference (1).

(4) S. B. Cohn, "Properties of Ridge Waveguide," Proc. IRE, Vol. 35,
     pp. 783-788, Aug. 1947.

(5) L. Young, "Tables for Cascaded Homogeneous Quarter Wave Trans-
     formers," Trans. IRE, Vol. MTT-7, pp. 233-237, April 1959.

(6) L. Young, "Correction to Tables for Quarter Wave Transformers,"
     Trans. IRE, Vol. MTT-8, pp. 243-244, March 1960.

(7) N. G. Sakiotis, A. J. Simmons, and H. N. Chait, "Microwave
     Antenna Ferrite Applications," Electronics, p. 156, June 1952.

Preceding page blank

APPENDIX A

IMPEDANCE MATCHING OBSERVATIONS

The significant differences of impedance between unloaded rec-
tangular waveguide and fully loaded quad ridged waveguide led to
considerable difficulty in matching one medium tᴏ the other. Because
of the considerable difficulties in employing tapered matching techniques
to commercially applicable phase shifters, quarter wave sections were
the only possibilities considered acceptable. To employ quarter
wave transformer techniques, impedance definitions must be uniformly
consistent. In any non-TEM structure, no unique definition of char-
acteristic impedance exists for the equivalent transmission line.
Three definitions of impedance are in common use, a V-I or voltage/
current definition, a V^2-P or voltage/power definition, and a P-I^2
or power/current definition. Herein we shall exclusively use the
former restricted even further so that V represents the maximum
voltage at the waveguide midpoint and I represents the total one way
current across the wall face. Thus, for the unloaded rectangular
waveguide

$$Z_0 = \frac{V}{I} = \frac{\int_0^b E_y \, (a/2 \; y) \; dy}{\int_0^a H_x \, (x,y) \; dx}$$

$$E_y = E_0 \sin (\pi x/a)$$

$$H_x = \frac{E_0}{Z_{TE}} \sin (\pi x/a)$$

Preceding page blank

$$Z_0 = \frac{\pi}{2} \frac{b}{a} \ Z_{TE} = \frac{\pi}{2} \frac{b}{a} \frac{n}{[\ 1-(f_c/f)^2]^{1/2}}$$

At S-band, for standard WR284 waveguide, Z_0 by this definition at 2GHz is 387.64Ω. For the ridged guide, Cohn (4) used a clever approach to approximate the characteristic impedance from a derived value far above cutoff. Again impedance definitions remain consistent and

$$Z = \frac{n}{[1-(\lambda/\lambda_c)^2]^{1/2}} \ \frac{2\pi b_0/\lambda_c}{C}$$

$$C \equiv \sin \frac{\pi a}{\lambda_c} + \frac{b_0}{b} \cos \frac{\pi a_0}{\lambda_c} \tan \frac{\pi(a-a_0)}{\lambda_c}$$

where a_0 is the width of the ridge and b_0 is the guide height between ridges or, equivalently, the ridge separation. When the double ridge waveguide geometry is distorted to create the quad ridge geometry, the characteristic impedance changes little and the impedance relation above was employed without modification. For the quad ridge geometries already described, the characteristic impedance falls between 62 and 71Ω calculated at 3 GHz. With the aid of the tables of Leo Young (5) interim impedance are easily specified. A significant problem yet remains, however, in translating the desired impedances into a physical design. For various reasons, centrally located dielectric plug loading of the rectangular waveguide was selected as the interim matching sections, and the impedance and guide wavelength of such sections must now be determined.

In the first efforts to specify impedance of a centrally located symmetric dielectric plug loaded waveguide, an effective dielectric constant was defined as an area weighted average.

$$\varepsilon_e = \frac{\varepsilon_1 A_1 + \varepsilon_2 A_2}{A_1 + A_2}$$

For the dielectric plug loaded waveguide as shown in Figure A.1, wherein A_1 is the area of the plug region and A_2 is the remaining unfilled area,

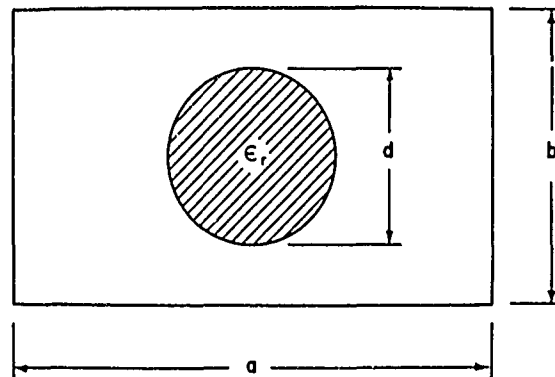$$\varepsilon_e = 1 + (\varepsilon_r - 1) \frac{\pi d^2/4}{ab} \qquad [A.1]$$

Figure A.1

Dimension Definitions for Dielectric Plug Loaded Waveguide

Impedance transformers were designed using normal waveguide formulas with ε replaced with the effective ε_e. The results, however, were disappointing and a cross check was made using the concept of an effective dielectric constant on the guide wavelength. Unfortunately, the addition of the dielectric plug means that the eigenvalues of the differential equation will no longer produce a propagation constant such that

$$\lambda g = \frac{\lambda}{[1-(\lambda/\lambda_c)^2]^{1/2}} \qquad [A.2]$$

However intuition hints that a cutoff frequency still exists, and furthermore that the guide wavelength varies as a function of this cutoff in some manner not dissimilar to that described above. To evaluate this functional relationship and to verify if this "effective dielectric constant" concept was usable, a sequence of guide wavelength tests were conducted on rectangular waveguide centrally loaded by circular dielectric rods of varying diameter. Tests were conducted at X-band using standard WR90 waveguide. Extra long dielectric rods of diameter .200, .250, and .300 were prepared using D13 material. The six inch long rods were centered in the waveguide using rexolite supports and matched at either end by D6 stubs of similar diameter. Measurements of wavelength was restricted to the central four inches of length of minimize measurement distortion caused by higher order modes close to the ends. Results are tabulated below.

D13 Rod Diameter (Inches)	Frequency (GHz)	Guide Wavelength (Centimeters)
0	8	6.48
0	9	4.66
0	10	3.94
.200	8	3.97
.200	9	3.18
.200	10	2.65
.250	8	2.82
.250	9 ·	2.07
.250	10	1.52
.300	8	1.92
.300	9	1.46
.300	10	1.17

Various possibilities exist to fit the measured data above to some variation of the basic form of equation [A.2]. It is possible, for example, to expect only λ_c to vary with dielectric loading perhaps by

$$\lambda_c \propto \sqrt{\varepsilon_e}$$

Solving for f_c in terms of λ_g shows that this is impossible. It is also possible to postulate λ_o as well as f_c to vary according to $\sqrt{\varepsilon_e}$ so that equation [A.2] becomes

$$\lambda_g = \frac{\lambda_o / \sqrt{\varepsilon_e}}{[1-(f_c/f)^2/\varepsilon_e]^{1/2}}$$

Once again, solving for f_c shows that such a form is improbable. Next, if one postulates that f_c varies differently than λ_o as a function of dielectric loading, then it is possible to determine both λ_e and f_c experimentally

$$\lambda_g = \frac{\lambda_0/\sqrt{\varepsilon_e}}{[1-(f_c/f)^2]^{1/2}}$$

[A.3]

Using data at 9 and 10 GHz to determine ε_e and then solving for f_c at all three frequencies leads to the results shown below.

D13 Rod Diameter (Inches)	Frequency (GHz)	ε_e	Calculated Cutoff Frequency
.200	8	2.060	6.04
.200	9		6.18
.200	10		6.18
.250	8	9.446	7.30
.250	9		7.69
.250	10		7.69
.300	8	12.381	6.68
.300	9		6.88
.300	10		6.88

Since the unloaded waveguide cutoff frequency for WR90 waveguide is 6.562, it was decided that for the purposes of the model, f_c would be considered a constant to be unaltered by the addition of dielectric loading. Then a new expression for effective dielectric constant was devised and has become a standard for subsequent characteristic impedance tests. Comparing with equations [A.1] it may be seen to differ by the addition of a cubic term

$$\varepsilon_e = 1 + (\varepsilon_r-1) \left[.95 \frac{\pi d^2/4}{ab} + 90 \left(\frac{\pi d^2/4}{ab}\right)^3\right]$$

Using this effective ε in the expression for waveguide impedance one obtains the equation

78

$$Z = \frac{\pi}{2} \frac{b}{a} \frac{\eta / \sqrt{\varepsilon e}}{[1-(f_c/f)^2]^{1/2}}$$

Transformers designed using this empirically selected formula did not fare well and some means of correlating this with actual characteristic impedances was sought. Thus the following test was devised using a Hewlett Packard Network Analyzer, Reflection Test Set, and Polar Display. A $\lambda/8$ section of dielectric loaded guide was formed by placing a circular stub on a shorting plate and placing it at the end of a waveguide. A sketch is shown in Figure A.2 along with an equivalent circuit. The transformed impedance of the short through the dielectric region with characteristic impedance Z_{01} is

$$Z_i = j \, Z_{01} \tan \beta_1 \ell_1$$

Since ℓ_1 is selected as $\lambda/8$, then $Z_i = j \, Z_{01}$. Naturally, impedance readings from the Network Analyzer are really reflection readings calibrated as VSWR and thus only an impedance ratio is available for calculation, but Z_0 of the unloaded guide is easily calculated so this presents no difficulty. The actual testing procedure involved four steps: 1) the correct length of dielectric rod was prepared for the diameter under test, 2) the number of unloaded waveguide wavelengths that this length represents was determined, 3) a short was placed on the unloaded waveguide and the display was rotated by reference until the short appeared advanced by the amount calculated in step 2, and 4) the shorting plate with the test stub in place was used as a shorting bar. In this way the reactance measurement re-
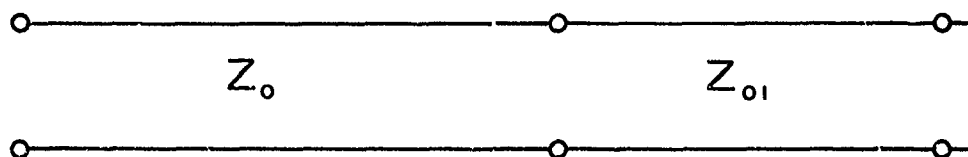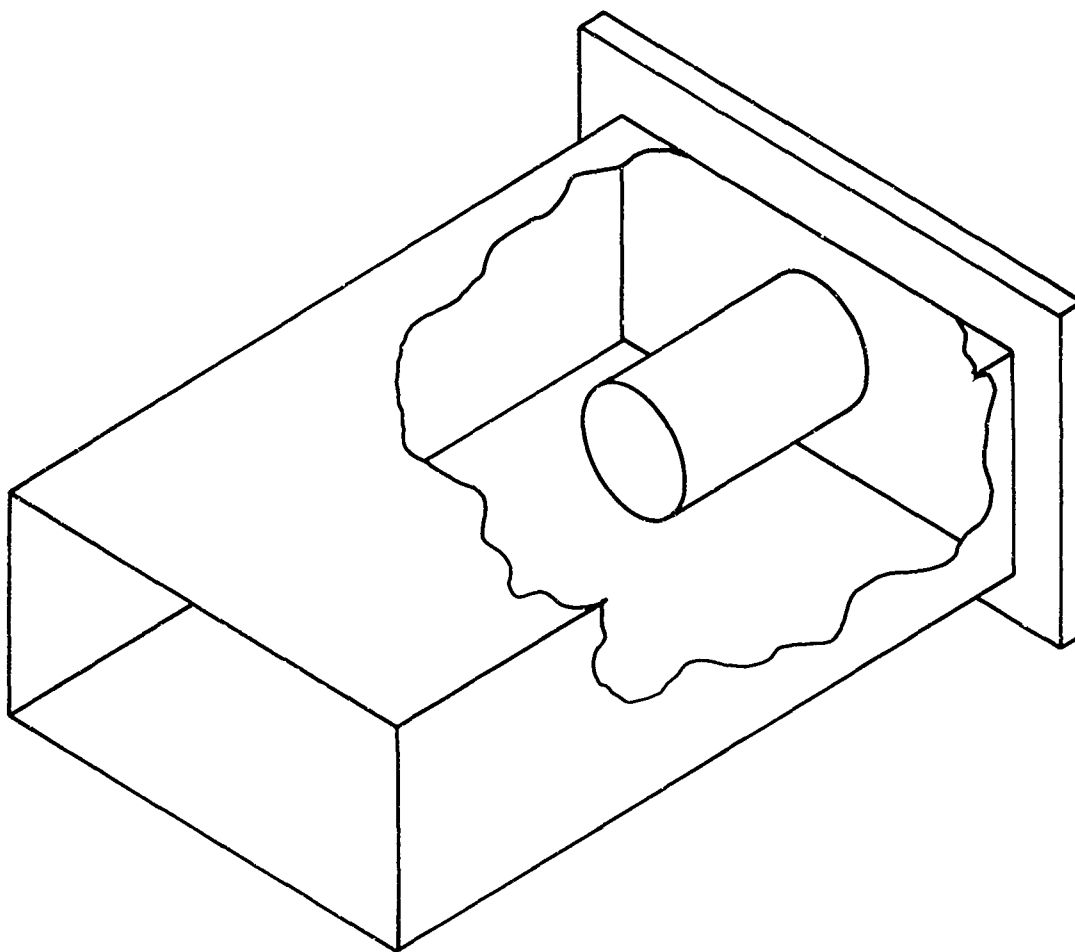
Figure A.2

Direct Impedance Measurement Configuration

presents exactly the desired impedance ratio Z_{01}/Z_0. Since guide wavelengths of dielectrically loaded waveguide were very accurately known at X-band, test evaluation began there. Test data is presented below, all measurements taken at 9 GHz.

Rod Diameter (Inches)	$\lambda/8$ Length (Inches)	λ/Length (Waveguide Wavelengths)	Observed Reactance (Ratio)	Z_0 (Ohms)
.200	.156	.0816 λ	.47	181 Ω
.250	.102	.0533 λ	.28	106 Ω
.300	.072	.0377 λ	.19	73 Ω

There is an inherent error in this type of measurement, because one term has thus far been ignored. At the junction between unloaded waveguide and plug-loaded waveguide a discontinuity exists that requires higher order modes in the junction vicinity in order to satisfy field boundary conditions. In the dominant mode equivalent circuit this may be represented by a shunt capacitive susceptance at the junction. The input admittance being measured is thus the sum of two terms only one of which is the desired characteristic admittance. The data is still useful, however, for it indicates general trends the model must follow and with the aid of this data the transformer matching technique as described in the text was eventually designed. Considering all the unanswered variables, however, it is felt that subsequent study is necessary before a definitive phenomenological model may be presented for consistently accurate synthesis.

APPENDIX B

SLOTLINE WAVELENGTH TESTS

To evaluate the phase velocity distinction between sandwich slotline (cf. Figure 3.1-b) and the 4 conductor slotline/microstrip composite (cf. Figure 3.1-3) the following guide wavelength tests were conducted.

Width of the slotline under test was 0.187 inch. The slotline was formed by silver deposit on garnet substrate. Garnet material was Xtalonix X805, similar in composition to TT G-800, with relative permittivity 14.7. Each slab of garnet forming the sandwich slotline was 0.125 inch thick, 6 inches in length and 2 inches wide. The center line of the microstrip launchers was placed 0.5 inch from each side leaving approximately a 5 inch region in which guide wavelength may be measured; only 3 inches of this length were utilized to avoid boundary condition evanescent modes near the launch discontinuity. The central conductors of balanced microstrip were introduced 0.5 inches from the launch centerline as shown in Figure B.1. Width of each balanced microstrip width was 0.8 inch.

Tests were conducted from 2.4 to 3.8 GHz on each of the two geometries, slotline only and slotline/microstrip. Below 2.4 GHz, magnetic loss of the garnet becomes prohibitive and above 3.9 GHz surface wave modes increase radiation loss. Examples of each phenomenon may be found in the semi-annual report [1], pp. 30-31.

Preceding page blank

Results are shown in Figures B.2 and B.3. These curves are almost identical. They seem to diverge at the lower frequencies, showing a 2.1% difference at 2.4 GHz and 7.8% difference at 2.5 GHz, but the difference quickly reduces to 22% and .00% at 2.6 and 2.8 GHz respectfully. The λ'/λ_0 ratio for this geometry varies slowly and is shown in Figure B.4.
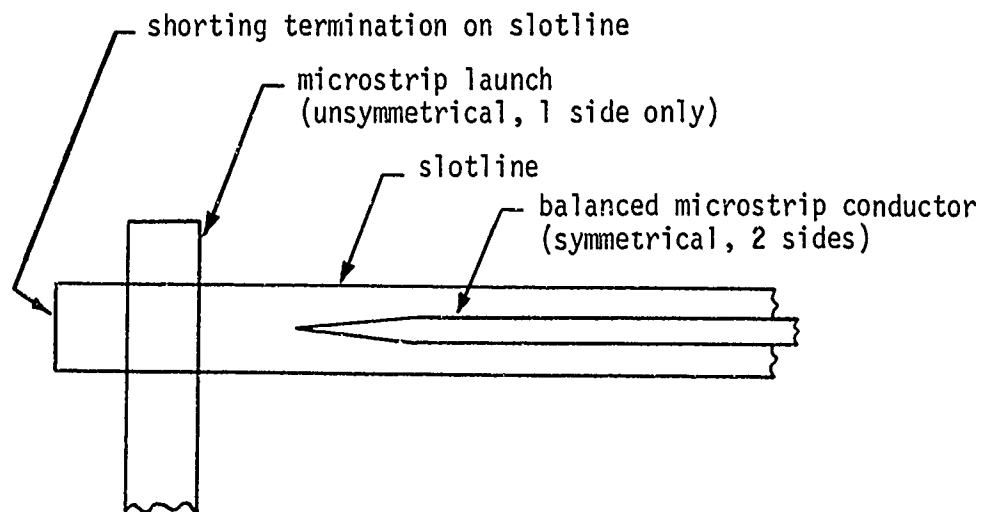

Figure B.1

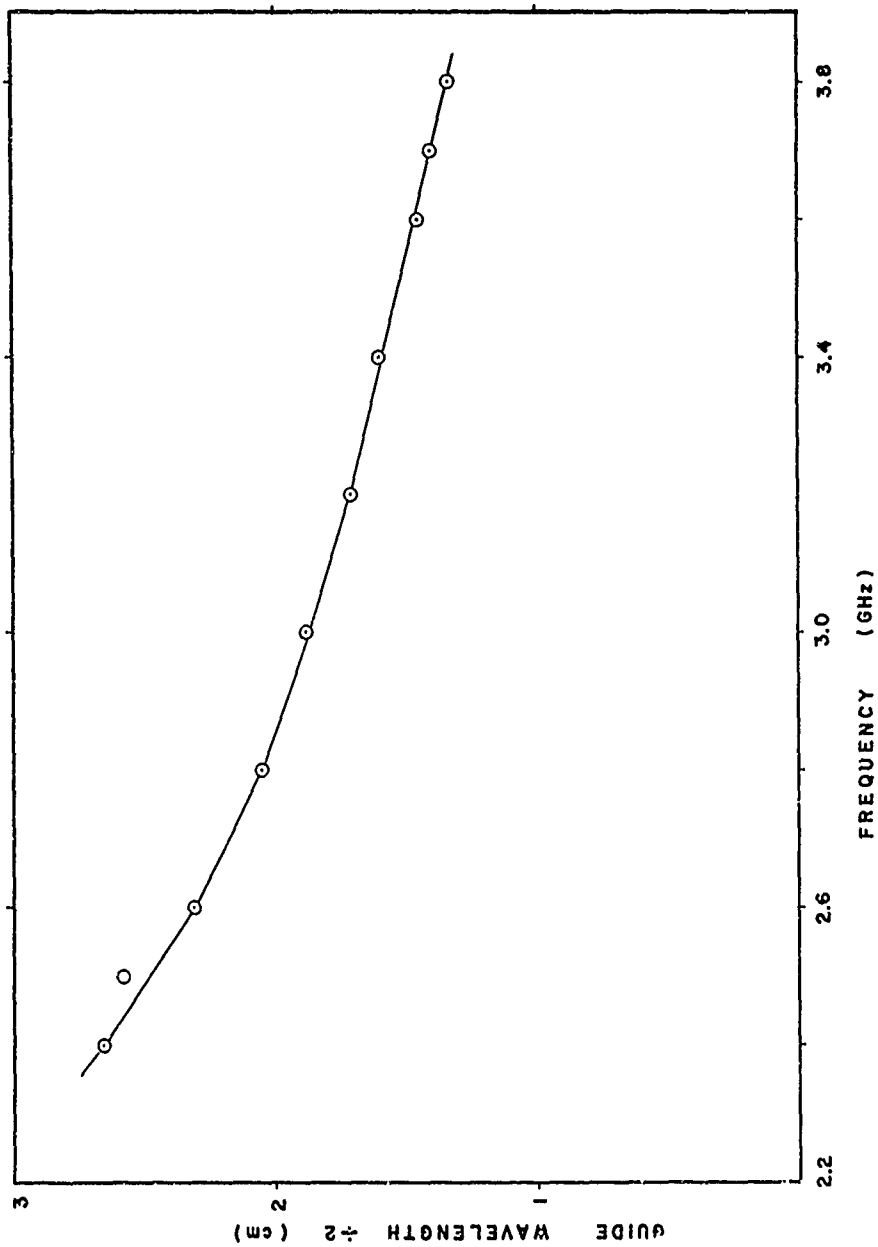Relative positions of principle conductors for guide wavelength tests.

Figure B.2

Guide wavelength of slotline. Experimentally measured wavelength at various frequencies, each point represents averaged data over 3 inches of length.
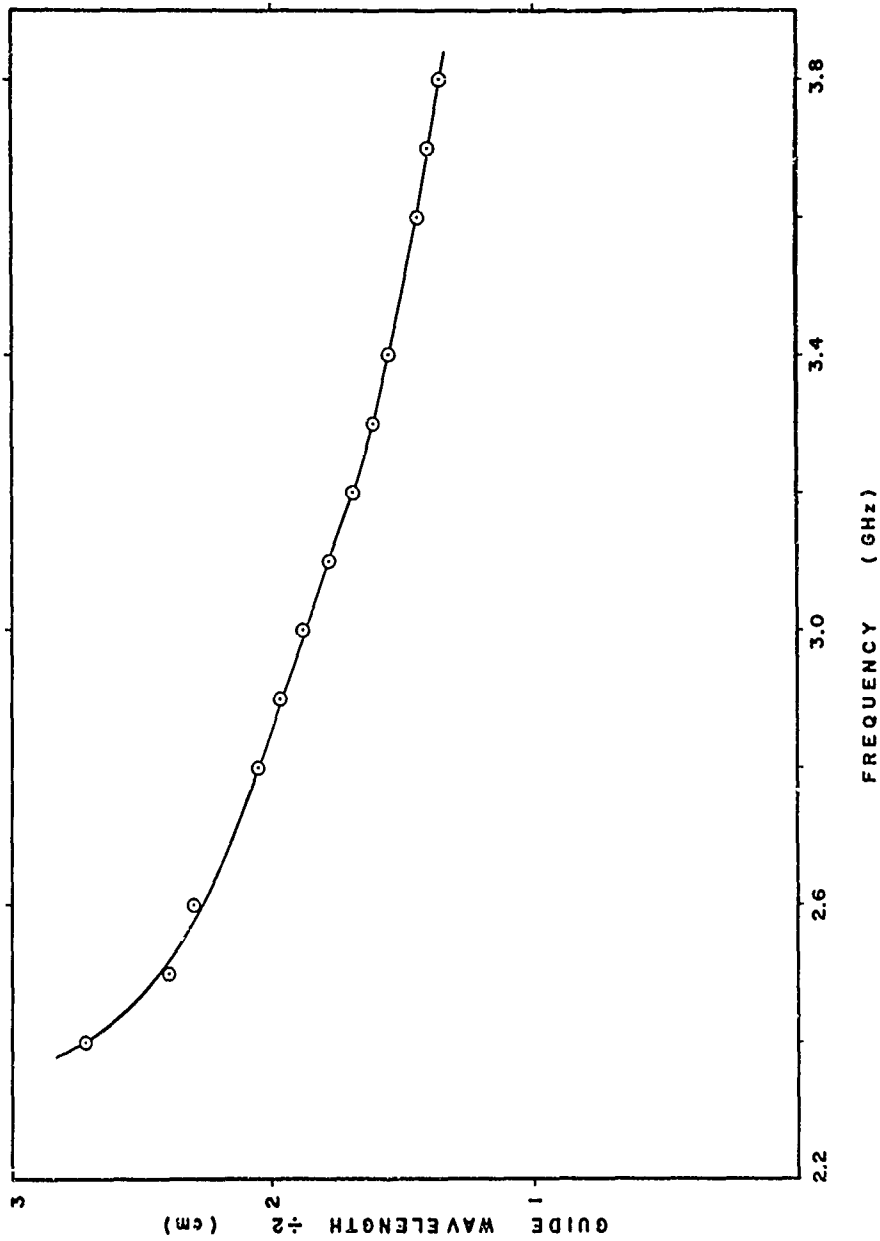
Figure B.3

Guide wavelength of slotline/microstrip propagating structure. Structure dimensions indicated in text.
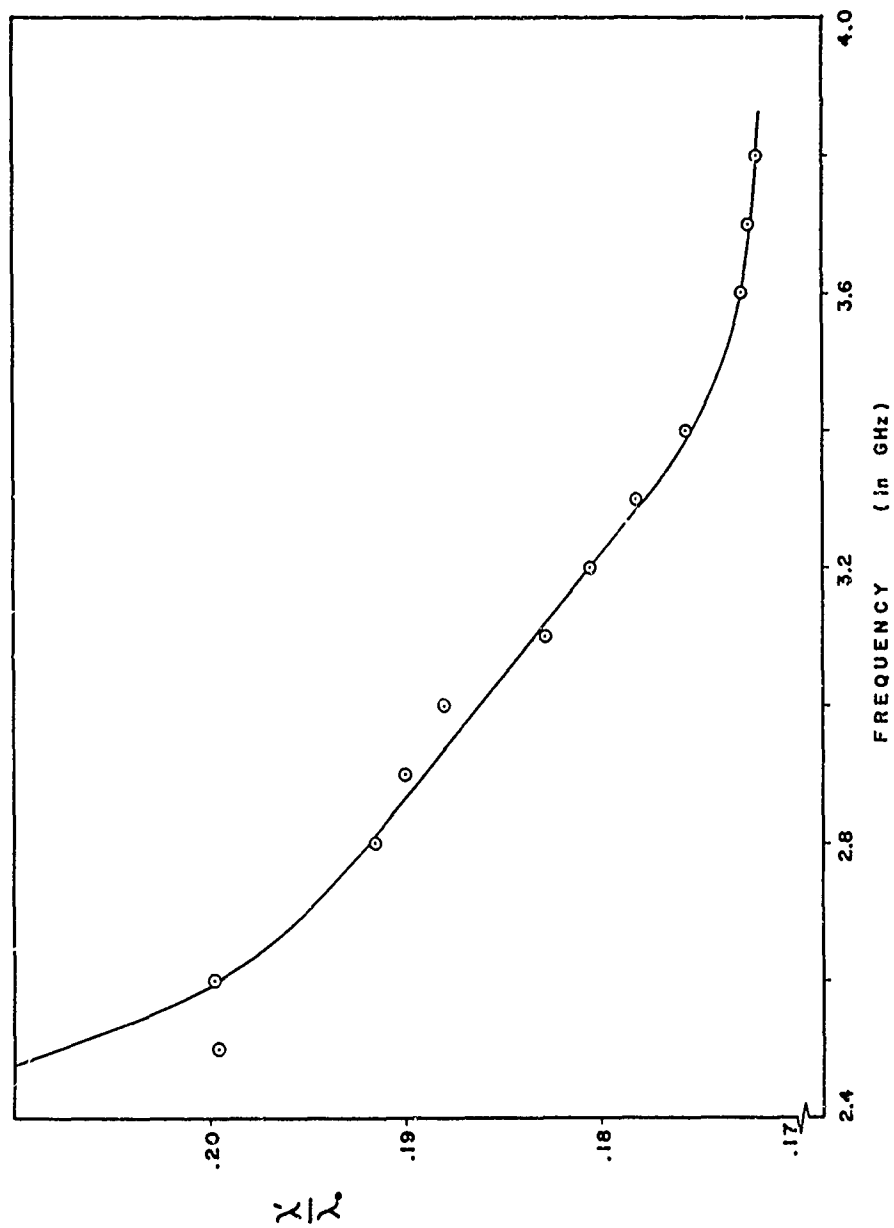
Figure B.4

Ratio λ'/λ_0 for sandwich slotline plotted as a function of frequency. This experimental data was for a slotline with $w/d = 1.5$ and $\epsilon_r = 14.7$.